HHS Public Access

Author manuscript

J Comp Neurol. Author manuscript; available in PMC 2018 May 01.

Published in final edited form as:

J Comp Neurol. 2017 May 01; 525(7): 1707–1730. doi:10.1002/cne.24166.

Somatic and neuritic spines on tyrosine hydroxylase–immunopositive cells of rat retina

Anna Fasoli[1], **James Dang**[1], **Jeffrey S. Johnson**[1], **Aaron H. Gouw**[1], **Alex Fogli Iseppe**[1], and **Andrew T. Ishida**[1,2]

[1]Department of Neurobiology, Physiology and Behavior, University of California, Davis, California

[2]Department of Ophthalmology and Vision Science, University of California, Sacramento, California

Abstract

Dopamine- and tyrosine hydroxylase–immunopositive cells (TH cells) modulate visually driven signals as they flow through retinal photoreceptor, bipolar, and ganglion cells. Previous studies suggested that TH cells release dopamine from varicose axons arborizing in the inner and outer plexiform layers after glutamatergic synapses depolarize TH cell dendrites in the inner plexiform layer and these depolarizations propagate to the varicosities. Although it has been proposed that these excitatory synapses are formed onto appendages resembling dendritic spines, spines have not been found on TH cells of most species examined to date or on TH cell somata that release dopamine when exposed to glutamate receptor agonists. By use of protocols that preserve proximal retinal neuron morphology, we have examined the shape, distribution, and synapse-related immunoreactivity of adult rat TH cells. We report here that TH cell somata, tapering and varicose inner plexiform layer neurites, and varicose outer plexiform layer neurites all bear spines, that some of these spines are immunopositive for glutamate receptor and postsynaptic density proteins (viz., GluR1, GluR4, NR1, PSD-95, and PSD-93), that TH cell somata and tapering neurites are also immunopositive for a γ-aminobutyric acid (GABA) receptor subunit ($GABA_AR_{\alpha 1}$), and that a synaptic ribbon-specific protein (RIBEYE) is found adjacent to some colocalizations of GluR1 and TH in the inner plexiform layer. These results identify previously undescribed sites at which glutamatergic and GABAergic inputs may stimulate and inhibit dopamine release, especially at somata and along varicose neurites that emerge from these somata and arborize in various levels of the retina.

Correspondence. Andrew Ishida, Department of Neurobiology, Physiology and Behavior, University of California, One Shields Avenue, Davis, CA 95616-8519. atishida@ucdavis.edu.

CONFLICT OF INTEREST

The authors declare no competing financial interests.

AUTHOR CONTRIBUTIONS

All authors had full access to all the data in the study and take responsibility for the integrity of the data and the accuracy of the data analysis. Study concept and design: ATI, AF. Acquisition of data: AF. Analysis and interpretation of data: AF, ATI, JSJ, JD, AFI, AG. Monte Carlo analysis and methods: JSJ. Drafting of the manuscript: ATI. Study supervision: ATI.

Keywords

retina; interplexiform cells; dopamine; dendrites; axons; spines; RRID: RGD_60991 (organism_-LErat); RRID: RGD_1566443 (organism_Lrat); RRID: AB_2201528 (antibody_TH MS); RRID: AB_90755 (antibody_TH_SH); RRID: AB_11001825 (antibody_PSD-93); RRID: AB_2307331 (antibody_PSD-95); RRID: AB_399431 (antibody_RIBEYE); RRID: AB_2213602 (antibody_GluR1); RRID: AB_90711 (antibody_GluR4); RRID: AB_2314955 (antibody_NMDAR1); RRID: AB_310272 (antibody_GABAA_α1); RRID: AB_2340863 (antibody_DKαMSaf647); RRID: AB_2315778 (antibody_DKαSHcy3); RRID: AB_2338694 (antibody_GTαIgG1MSCy3); RRID: AB_2338917 (antibody_GTαIgG2aMSaf647); RRID: AB_2576217 (antibody_GTαRBaf488); RRID: AB_2338854 (antibody_GTαIgG1MSaf488); RRID: SCR_002285 (Fiji); RRID: SCR_014237 (Huygens); RRID: SCR_007370 (Imaris); RRID: SCR_001622 (MatLab); RRID: SCR_001905 (R Project for Statistical Computing); RRID: NLX_143660 (database_JCNantibody)

1 | INTRODUCTION

Of the many interneurons that vertebrate retinae use to modulate visually driven signal generation, spread, and transmission (Marc, 2008), the first histochemically identified types were found to be catecholaminergic (Häggendal & Malmfors, 1965), bind antibodies directed against tyrosine hydroxylase (TH) (Nguyen-Legros, Berger, Vigny, & Alvarez, 1981), and emit neurites that arborize in the inner and outer plexiform layers (Ehinger & Falck, 1969). These interneurons (termed TH cells hereafter) are found in all vertebrate classes and are thought to contribute to light adaptation of the retina and pigment epithelium (Witkovsky & Dearry, 1991) by releasing dopamine during illumination (Kramer, 1971; Brainard & Morgan, 1987).

Previous studies have hypothesized that TH cells release dopamine from varicose axons after excitatory synapses depolarize TH cell dendrites in the inner plexiform layer and these depolarizations spread radially to the varicosities (Dacey, 1990; Witkovsky, Gábriel, & Krizaj, 2008). Although anatomical, electrophysiological, and imaging observations are consistent with radially spreading depolarizations in some medium- and wide-field amacrine cells (Famiglietti, 1991; Taylor, 1996; Euler, Detwiler, & Denk, 2002; Davenport, Detwiler, & Dacey, 2007), it is less clear how the structural compartments of TH cells function. For example, although varicosities in TH cell neurites form synapses onto other neurons (Pourcho, 1982; Holmgren, 1982; Voigt & Wässle, 1987; Kolb, Cuenca, Wang, & Dekorver, 1990; Kolb, Cuenca, & Dekorver, 1991; van Haesendonck, Marc, & Missotten, 1993; Contini & Raviola, 2003), dopamine release has been detected only from TH cell somata (Puopolo, Hochstetler, Gustincich, Wightman, & Raviola, 2001). Similarly, although dopamine release can be blocked by a voltage-gated Na^+ channel toxin (Puopolo et al., 2001; see also Piccolino, Witkovsky, & Trimarchi, 1987) and can be reduced by Ca^{2+} channel toxins and heavy metals (Sarthy & Lam, 1979; Frederick, Rayborn, Laties, Lam, & Hollyfield, 1982; Kolbinger & Weiler, 1993; Tamura et al., 1995; Boelen, Boelen, & Marshak, 1998), antibodies directed against voltage-gated Na^+ and Ca^{2+} channels bind to neurites in the inner plexiform layer but not in the outer plexiform layer (Xu, Zhao, & Yang, 2003; Witkovsky et al., 2004; Witkovsky, Shen, & McRory, 2006; Witkovsky et al., 2008). For that matter, TH has been found to colocalize with synaptic vesicle- and release-related

proteins in the inner plexiform layer, but in only some varicosities within the inner nuclear layer and not in the outer plexiform layer (Witkovsky et al., 2004, 2008; Witkovsky, Arango-Gonzalez, Haycock, & Kohler, 2005). Additionally, TH cells have been reported to differ at the level of their postsynaptic architecture. In particular, dendritic spine-like appendages have been found on TH cell dendrites in some species, but not on dendrites in other species, and also not on somata that release dopamine when exposed to glutamate receptor agonists (Dacey, 1990; Teakle, Wildsoet, & Vaney, 1984; Kolb et al., 1990; Tauchi, Madigan, & Masland, 1990; Gábriel, Zhu, & Straznicky, 1992; Guimarães & Hokoç, 1997; Puopolo et al., 2001).

It is possible that TH cells release dopamine by different mechanisms in the inner and outer plexiform layers, and that TH cell shape and ion channel distribution vary with species. However, most studies to date have examined TH cells in retinae that were incubated in aldehyde-based fixatives that we have found to deform, and reduce the detectability of, retinal ganglion cell axons and dendrites (Stradleigh, Greenberg, Partida, Pham, & Ishida, 2015). The present study examines the shape, contour, and immunostaining of TH cells by use of protocols we developed to preserve the dendritic and axonal morphology of proximal retinal neurons and to localize transmembrane and membrane-associated proteins (Stradleigh et al., 2011, 2015).

2 | MATERIALS AND METHODS

2.1 | Animals

Adult rats were used for this study based on previous descriptions of their TH cell morphology and immunostaining (Ngyuen-Legros et al., 1981; Voigt & Wässle, 1987; Savy et al., 1995; Witkovsky, Arango-Gonzalez, Haycock, & Kohler, 2005; Witkovsky et al., 2008). Long–Evans and Lewis rats (female and male; P60–P120; 150–250 g; RRID: RGD_60991, RRID: RGD_1566443) were obtained from a commercial supplier (Harlan Bioproducts, San Diego, CA) and housed in standard cages at ~23 °C on a 12-hr/12-hr light/dark cycle. The Lewis rats were used to test whether spine numbers and immunostaining patterns differed between inbred and outbred strains. We found no significant or consistent difference between these properties in these strains and, therefore, pool the results below. The morphometric observations reported here (Figures 1–5) were collected from Long–Evans rats ($n \geq 3$ rats for each measurement or observation). Each rat was anesthetized by intraperitoneal (i.p.) ketamine and xylazine (70–100 mg/kg and 5–10 mg/kg, respectively; see below for the source of chemicals used in this study), enucleated, and killed by a lethal dose of sodium pentobarbital (150 mg/kg, i.p.). Before enucleation, the superior side of each eye was marked for quadrant identification during data analysis. All animal care and experimental protocols were approved by the Animal Use and Care Administrative Advisory Committee of the University of California, Davis.

2.2 | Fixation and immunohistochemistry

In most experiments, each enucleated eye was hemisected in oxygenated Ames solution at room temperature. For comparison, some eyes were hemisected in ice-cold, sucrose-

supplemented phosphate buffer (PB) (Stradleigh et al., 2015). After removal of the vitreous, the resulting eyecups were processed as either whole mounts or vertical sections.

To form flat mounts, the retina was isolated with forceps, placed photoreceptor-side down on a membrane filter (PICM0RG50, Millicell; Millipore, Tuliagreen, Ireland), and immersed in a prefixative conditioning solution containing sucrose (200 mM) for an additional 30 min (Stradleigh et al., 2015). Although this solution was ice-cold in most experiments, similar results were obtained when it was room temperature or even warmed to 37 °C. Membrane-attached retinae were then fixed either overnight at 4 °C, or for 20 min at room temperature, in a fixative containing formaldehyde (4% w/v) and sucrose (200 mM) in 100 mM 4-(2-hydroxyethyl)-1-piperazine-ethanesulfonic acid (HEPES) (Stradleigh et al., 2015; cf. Stell & Lightfoot, 1975; Anderson et al., 2009; Pallotto, Watkins, Fubara, Singer, & Briggman, 2015). In comparison experiments, sucrose was not included in the conditioning solution or fixative, and the fixative contained formaldehyde (4% w/v) in phosphate-buffered saline (PBS; 154 mM NaCl, 3.23 mM Na_2HPO_4, and 1.05 mM KH_2PO_4). The membrane-attached retinae were then rinsed in a Tris–Triton solution (100 mM Tris-HCl, 0.1% v/v Triton-X100, 0.01% w/v sodium azide, pH 7.5), and blocked and permeabilized overnight at 4 °C in the same solution supplemented with bovine serum albumin (BSA; 2% w/v) and either normal donkey or normal goat serum (5% v/v). The retinae were then incubated in primary antibodies (overnight at 37 °C after the overnight fixations, 3–4 days at 4°C after the 20-min fixations), rinsed in Tris–Triton, and incubated in secondary antibodies overnight at 4 °C. Primary antibodies were diluted in Tris–Triton supplemented with BSA (2% w/v). To help locate the outer nuclear, inner nuclear, and ganglion cell layers, preparations were counterstained with TO-PRO-3 (1:3,000) after secondary antibody incubation.

To form vertical sections, eyecups were passed through the conditioning and fixative solutions listed above. The fixed retinae were then isolated from each eyecup, rinsed in Tris–Triton (pH 7.5), embedded in 5% (w/v) low-melt agarose at 37 °C, allowed to set for 30–60 min at 4 °C, and cut into blocks with a razor blade. These blocks were sectioned vertically at a thickness of 100 μm on a vibrating microtome (VT1000S; Leica Microsystems, Wetzlar, Germany). Free-floating sections were blocked and permeabilized for 24 hr at 4 °C in Tris–Triton (pH 7.5) supplemented with 0.5% BSA and 5% normal goat serum. The sections were incubated in primary antibody overnight at 4 °C, rinsed with Tris–Triton, and incubated in secondary antibody overnight at 4 °C. 4’,6-Diamidino-2-phenylindole (DAPI; 1:3,000) was used as a nucleic acid counterstain and applied to tissue after secondary antibody incubation.

After rinsing, flat mounts and vertical sections were mounted directly to glass coverslips (No. 1.5), covered with a CUBIC/2 solution (refractive index = 1.49; Susaki et al., 2015) or with FluorSave mounting medium, and secured onto glass slides.

2.3 | Antibody characterization

Table 1 lists the primary antibodies used in this study. Each is listed in *The Journal of Comparative Neurology* Antibody Database V.14 (http://onlinelibrary.wiley.com/journal/10.1002/(ISSN)1096-9861/homepage/jcn_antibody_database.htm, RRID:NLX_143660).

The mouse monoclonal anti-TH antibody (Chemicon, Temecula, CA; Cat# MAB318; clone LNC1, RRID: AB_2201528) was generated against tyrosine hydroxylase purified from PC12 cells and diluted 1:1,000. This antibody has been characterized by immunohistochemistry in rat retina (Partida, Lee, Haft-Candell, Nichols, & Ishida, 2004; Witkovsky et al., 2008).

The sheep polyclonal anti-TH antibody (Chemicon; Cat# AB1542; RRID: AB_90755) was generated against native TH from rat pheochromocytoma and diluted 1:500. This antibody has been characterized by immunohistochemistry in mouse retina (Keeley & Reese, 2010).

The mouse monoclonal anti-postsynaptic density protein 95 (PSD-95) antibody (UC Davis/NIH NeuroMab Facility, Davis, CA; Cat# 75-028, clone K28/43, RRID: AB_2307331) was generated against fusion protein amino acids 77–299 (PDZ domains 1 and 2) of human PSD-95, and diluted to 0.2 μg/ml. This antibody has been characterized by immunoblotting and immunohistochemistry in chick retina (Wahlin, Moreira, Huang, Yu, & Adler, 2008).

The mouse monoclonal anti-PSD-93 antibody (UC Davis/NIH NeuroMab Facility; Cat# 75-284, clone N18/28, RRID: AB_11001825) was generated against fusion protein acids 1–852 (full-length) of rat Chapsyn-110, and diluted to 0.2 μg/ml. This antibody has been characterized by western blotting of mice cerebellar lysates and immunohistochemistry of mouse cerebellar Purkinje cells (Liu, Lee, & Ackerman, 2015).

The rabbit polyclonal anti-GluR1 antibody (Chemicon; Cat# AB1504; RRID: AB_2213602) was generated against a KLH-conjugated linear peptide corresponding to the C-terminal sequence of human glutamate receptor 1, and diluted to 0.2 μg/ml. This antibody has been characterized by immunoblotting in rat brain (Wenthold, Yokotani, Doi, & Wada, 1992).

The rabbit polyclonal anti-GluR4 antibody (Chemicon; Cat# AB1508; RRID: AB_90771) was generated against a linear peptide corresponding to the C-terminal sequence (RQSSGLAVIASDLP) of rat glutamate receptor 4, and diluted to 1 μg/ml. This antibody has been characterized by immunoblotting in rat brain (Wenthold et al., 1992).

The rabbit monoclonal anti-NR1 antibody (Chemicon; Cat# AB9864) was generated against a synthetic peptide corresponding to amino acids 909–938 of rat N-methyl-D-aspartate receptor 1 (NMDAR1) receptor subunit and diluted 1:500. This replaces Chemicon #AB1516 (RRID: AB_2314955), which has been characterized by western blotting and immunohistochemistry in rat retina (Fletcher, Hack, Brandstätter, & Wässle, 2000; Gründer, Kohler, & Guenther, 2000; Zhang & Diamond, 2006).

The rabbit polyclonal anti-γ-aminobutyric acid A receptor α1 ($GABA_AR_{\alpha 1}$) antibody (Upstate Biotechnology, Lake Placid, NY; Cat# 06-868, RRID: AB_310272) was generated against a KLH-conjugated linear peptide corresponding to the topological domain of rat $GABA_A$ receptor α1 subunit, and diluted to 0.5 μg/ml. This antibody has been characterized by immunohistochemistry in rabbit retina (Chen & Chiao, 2008).

The mouse monoclonal anti-C-terminal binding protein 2 (CtBP2, RIBEYE; BD Biosciences, San Jose, CA; Cat# 612044, clone 16/CtBP2; RRID: AB_39941) antibody was generated against the C-terminal amino acids 361–445 of mouse CtBP2, and diluted to 0.5 μg/ml. This antibody has been characterized by immunoblotting and immunohistochemistry in mouse retina (tom Dieck et al., 2005).

Signals attributed to the primary antibodies were visualized with donkey or goat, species- and subclass-specific, fluorophore-conjugated secondary antibodies (Jackson ImmunoResearch, West Grove, PA; Cat# 115-165-205, 115-545-205, 115-605-206, 713-165-147, 715-485-151, 715-605-151; ThermoFisher Scientific, Pittsburg, PA; Cat# A-11034), all diluted in Tris–Triton (typically at 1:500 dilution). The fluorophores were DyLight488, Alexa Fluor 488, Cy3, or Alexa Fluor 647.

2.4 | Confocal imaging

Confocal images were acquired on laser scanning confocal microscopes. One imaging system was a FluoView FV1000 Confocal System (version 1.6, Olympus, Center Valley, PA) interfaced to an Olympus IX-81 inverted microscope. Excitation was provided by Ar (488 nm), green He–Ne (543 nm), and red He–Ne (633-nm) lasers. Data were collected using an oil immersion 40 × objective (numerical aperture = 1) and a 60 × objective (numerical aperture = 1.42) in series of optical sections at step sizes of 0.220 μm, with two- or three-frame Kalman averaging for each section. The refractive index of the immersion oil (Cargille, Cedar Grove, NJ; Type LDF, Cat# 16241) was 1.515. Low-magnification images of whole retinae were collected with a 4 × objective with 2 × digital zoom.

The other imaging system was a Leica TCS SP8 high-sensitivity confocal microscope, coupled with Leica Application Suite X software (Leica Microsystems, Buffalo Grove, IL). Excitation was provided by a white light laser with up to eight excitation lines between 470 and 670 nm. Data were collected using an oil immersion 63 × objective (numerical aperture = 1.4) and a 100 × objective (numerical aperture = 1.4) in series of optical sections at step sizes of 0.180 μm, with eight-frame Kalman averaging for each section. The refractive index of the immersion oil (Leica Microsystems; Type F, Cat# 11513859) was 1.518.

Data that were subsequently deconvolved (see below) were oversampled by use of an oil immersion 60 × objective with 2.5 × digital zoom, or an oil immersion 100 × objective. The step size for the z-stacks ranged from 0.150 to 0.20 μm, resulting in voxel dimensions ranging from 0.072 to 0.088 μm for the x and y dimensions, and from 0.150 to 0.20 μm for the z dimension.

2.5 | Data analysis

Data sets were imported into the ImageJ package Fiji (http://imagej.net/Fiji, RRID: SCR_002285). If needed, adjacent optical sections were merged in the z-axis to form a projected image (using Fiji) or in the x–y plane to form a montage (using the grid stitching plug-in in Fiji; Preibisch, Saalfeld, & Tomancak, 2009). Somatic diameter was determined by tracing a polygon around the perimeter of the cell body, and averaging the maximum and minimum Feret's diameters calculated with Fiji. An area termed "dendritic field" in other studies was calculated from the polygon formed by straight lines connecting the distalmost

ends of the tapering neurites (Lin & Masland, 2006). Cell density was measured as the number of TH cell somata within a 1-mm^2 square patch of retina. The cell densities reported here showed no dependence on the orientation of these squares (e. g., whether the side or a corner of the square faced the optic disc). Coverage factors were calculated as the product of dendritic field area and cell density (Cleland, Levick, & Wässle, 1975) for comparison with results of other studies. Because we found that TH cell density varies with quadrant and eccentricity (see Results), we used the cell density for the 1-mm^2 patch of retina centered around each cell studied. The 3D reconstructions of processes and spines were performed using the Filament Tracer tool in Imaris (Bitplane, Zurich, Switzerland, RRID: SCR_007370). Reconstructions of somata used the Surface tool in Imaris.

Changes in color space, adjustments to brightness or contrast (if any), and image overlays were made in Photoshop CS6 (Adobe Systems, San Jose, CA). Statistical analyses were performed using Excel 2013 (Microsoft, Redmond, WA) and R (https://www.R-project.org/; RRID: SCR_001905). Data are presented as mean ± standard error of the mean (*SEM*). The statistical analysis of data groups shown in Figure 4E was performed using a one-way analysis of variance (ANOVA) followed by Tukey's post hoc test, whereas comparisons of two groups in Figure 4F were made using unpaired Student's *t* test. The significance level was set at a p value < .05.

2.6 | Deconvolution

An iterative algorithm (Classic Maximum Likelihood Estimation; https://svi.nl/MaximumLikelihoodEstimation) in the Huygens Professional image processing software of Scientific Volume Imaging (Hilversum, The Netherlands), and point spread functions (PSF) for our confocal imaging systems, were used to deconvolve digitally acquired images of TH cells. The PSFs were generated by the Huygens software based on the parameters of the microscope in each confocal imaging system. These were as effective as PSFs estimated from optical sections of fluorescent beads in generating restored images.

2.7 | Statistical analysis of colocalization

A Monte Carlo permutation analysis (10,000 repeats) was performed in MatLab (Mathworks, Natick, MA; RRID: SCR_001622) on cell images ($n = 4$) to test the null hypothesis that the observed colocalization of TH and GluR1 occurred by chance. In each image, the centers of the GluR1 spots were located in 3D space (G_{xyz}), and the numbers of points in G_{xyz} within 0.2 μm of the TH-stained cell were counted (observed count [O_c]). For each of the 10,000 repeats, a random set of locations R_{xyz} (having the same number of elements as G_{xyz}) was generated within the image volume by randomly associating, without replacement, the values in G_x, G_y, and G_z. From each R_{xyz}, the randomized locations (R_c) within 0.2 μm of the TH-stained cell were counted. The p value of this analysis was taken as the probability that R_c exceeded or was equal to O_c. p values below 0.05 were interpreted as rejecting the null hypothesis.

2.8 | Reagents

Reagents were obtained from the following sources: Abbott (Chicago, IL): sodium pentobarbital (0074-378-05); Affymetrix (Santa Clara, CA): low melt agarose (32829),

HEPES, (pH 7.3, 16924); Calbiochem (San Diego, CA): FluorSave (345789); Corning (Corning, NY): Tris-HCl, pH 7.5 (46-030CM); Fisher Scientific (Pittsburgh, PA): PBS (Ca^{2+}- and Mg^{2+}-free, pH 7.4; MT21040CV); Invitrogen (Grand Island, NY): DAPI (D21490); Jackson ImmunoResearch: normal donkey serum (017000121), normal goat serum (005000121); Sigma-Aldrich (St. Louis, MO): BSA (A8806), sodium azide (S2002); Thermo Fisher Scientific: TO-PRO-3 (T3605), Triton X-100 (BP151-100); United States Biological (Salem, MA): Ames (A1372-25); Western Medical Supply (Arcadia, CA): ketamine (4165), xylazine (5533).

3 | RESULTS

This study used immunohistochemistry, laser scanning confocal microscopy, and deconvolution of optical sections to characterize the shape, dimensions, distribution, and synapse-related immunoreactivities of TH-immunopositive adult rat retinal cells (referred to hereafter as TH cells). The results are arranged below to (a) compare TH cell neurites in retinae processed by different fixation protocols; (b) examine TH cell morphometrics and distribution under conditions that preserve the shape and contour of these and other neurites; and (c) describe the presence and immunostaining of spines in the somata and neurites of TH cells. As in other species (Mariani & Hokoç, 1988; Mitrofanis, Vigny, & Stone, 1988; Crooks & Kolb, 1992; Eglen, Raven, Tamrazian, & Reese, 2003; Tauchi et al., 1990), most of the TH cell somata in our preparations were brightly immunofluorescent whereas others were conspicuously dimmer (Figure 3). The data and observations reported here were collected from cells with bright somata only. We occasionally observed dimly fluorescing neurites intermingled with brightly fluorescing neurites (not illustrated). We presume that the former emerged from dim somata as in other species (Mariani & Hokoç, 1988; Tauchi et al., 1990) and did not attempt to collect data from them.

3.1 | TH cell neurites

Most previous studies have immunostained TH cells in retinae fixed by immersion in formaldehyde (FA) diluted to 4% w/v in PB or PBS. Because we have found that retinal ganglion cell dendrites and axons deform during immersion in 4% FA (Stradleigh et al., 2015) and that preincubation in a fixative-free medium and use of sucrose-supplemented FA preserves the shape and contour of dendrites and axons (Stradleigh et al., 2015), we compared the morphology of TH cells in retinae incubated in 4% FA versus those in retinae preincubated in sucrose-supplemented HEPES solution (or, with no noticeable difference, sucrose-supplemented PB) and then fixed in FA diluted to 4% w/v in sucrose-supplemented HEPES. We refer to this latter protocol hereafter as fixation in sucrose-supplemented FA without mentioning the preincubation.

Preparations fixed in sucrose-supplemented FA showed two types of neurites extending away from the TH cell somata (Figures 1–12). Some were ~2 μm in diameter where they emerged, tapered gradually to ~1 μm, were smoothly contoured except for the presence of spines (see below), and branched as many as four times along their length. The others emerged from somata (or, in some cases, from larger caliber, gradually tapering processes; see Figures 1–6), tapered within a short distance to a thin diameter (roughly 0.6 μm), were

decorated with varicosities and spines, and branched rarely (if at all). In retinae fixed in sucrose-supplemented FA, TH cells present tapering and varicose neurites, and retinal ganglion cell dendrites and axons are spared from artifactual formation of varicosities (cf. Stradleigh et al., 2015).

The tapering neurites of TH cells fixed in sucrose-supplemented FA ranged in length from 25 to 393 μm. Polygons formed by straight lines connecting the tips of the tapering neurites of individual cells ranged in shape from ovate to oblong (Figure 2). We found no tendency of the long axes of these fields to orient in particular directions relative to the ganglion cell axon fascicles heading toward the optic disc. The areas of the polygonal fields varied with retinal position, from ~0.04 mm^2 in the superior retina roughly half way between the optic disc and the retinal periphery, to ~0.10 mm^2 in the retinal periphery. In the superior retina, the averages of the long and short axis lengths of these fields measured 530 ± 82 μm and 330 ± 54 μm (mean ± *SEM, n* = 11), respectively, and the areas of the polygons ranged from 0.035 to 0.080 mm^2. In the inferior retina, the averages of the long and short axis lengths of these fields measured 1,073 ± 176 μm and 478 ± 93 μm (mean ± *SEM, n* = 6), and the areas of the polygons ranged from 0.042 to 0.158 mm^2. The average of all of the areas we measured was 0.074 ± 0.008 mm^2 (mean ± *SEM, n* = 17; median: 0.066 mm^2).

The varicose neurites of TH cells fixed in sucrose-supplemented FA extended laterally in multiple directions well beyond the polygonal fields described above. Due to their length, these neurites overlapped neurites of other TH cells to the extent that we typically could not measure the full length of individual varicose neurites or the areas of the fields they formed (e. g., Figure 1C). On occasion, we were able to follow the arborization of single varicose neurites for more than 100 μm (Figures 2–3, and 7).

Long, tapering TH-immunopositive neurites were not found in preparations fixed in straight 4% FA. The inner plexiform layer was, instead, cluttered with many spots and short, heavily beaded segments of TH-immunopositive processes (Figure 1A and B). The position of these spots and segments (especially between TH-immunopositive somata in the inner plexiform layer) suggests they are either neurites that fragmented into disconnected TH-immunopositive pieces or TH-immunopositive neurites in which many short segments failed to display TH immunoreactivity. The remaining data of this study were collected only from preparations fixed in sucrose-supplemented FA.

3.2 | Cell types

Most of the TH cell somata in our preparations were found at the edge of the inner nuclear layer immediately adjacent to the inner plexiform layer (Figure 3). As in other species (Ehinger & Falck, 1969; Nguyen-Legros et al., 1981; Oyster, Takahashi, Cilluffo, & Brecha, 1985; Voigt & Wässle, 1987; Guimarães & Hokoç, 1997; Eglen et al., 2003), some TH cell somata were found either in the ganglion cell layer or, rarely, within the inner plexiform layer (Figure 3B and C). The diameters of the inner nuclear layer somata (calculated as the average of the short and long axes for each cell viewed in retinal flat mounts) ranged from 11.2 to 17.3 μm (mean ± *SEM*: 14.2 ± 0.1 μm, *n* = 155; Figure 3G) and did not significantly differ from a normal distribution (Figure 3G, inset). The diameters of the ganglion cell layer somata ranged from 16.2 to 21.7 μm (mean ± *SEM*: 18.4 ± 0.4 μm, *n* = 19).

TH cell neurites arborized in the most distal (i. e., sclerad) and most proximal (i. e., vitread) sublaminae of the inner plexiform layer, and in the sublamina intermediate between these. For comparison with previous studies, these will be referred to as s1, s5, and s3, respectively. Varicose neurites also projected distally through the inner nuclear layer and arborized laterally within the outer plexiform layer. The neurites ramifying in the inner and outer plexiform layers will be referred to as internal and external neurites, respectively (cf. Savy et al., 1995). Some external neurites were seen projecting from somata in the inner nuclear layer toward the outer plexiform layer (Figure 3A and D), and TH-immunopositive neurites were seen arborizing in the outer plexiform layer in all retinal quadrants. Based on previous descriptions (Nguyen-Legros et al., 1981; Savy et al., 1995; Witkovsky et al., 2005, 2008), we interpret these somata and neurites as belonging to interplexiform cells. Although interplexiform TH cells are found only in the inferior retina of some species (rabbit: Oyster et al., 1985; cat: Kolb et al., 1990), external projections of interplexiform TH cells have been found in all quadrants of rat and *Xenopus* retinae (Savy et al., 1995; Witkovsky, Zhang, & Blam, 1994) and we have found TH-immunopositive neurites interconnecting the inner and outer plexiform layers in both superior and inferior retinae (Figures 3A, 3D, and 12). Segments of TH-immunopositive neurites were occasionally found in the outer nuclear layer, although these were too rare to study in any detail (not illustrated; cf. Negishi et al., 1985; Nguyen-Legros, Moussafi, & Simon, 1990; Gábriel, Zhu, & Straznicky, 1991; Savy et al., 1995).

Ascending processes were not observed on some somata, as might be expected of amacrine TH cells. However, this does not exclude the possibility that these are interplexiform cells, because previous studies have shown that ascending processes of some cells emerge from the inner plexiform layer (Ehinger & Falck, 1969; Oyster et al., 1985; Kolb et al., 1990; Dacey, 1990; Savy et al., 1995; van Haesendonck et al., 1993). We know of no methods that would distinguish all of the amacrine cells from the interplexiform cells in individual retinae. It is also not known whether TH somata in the inner plexiform and ganglion cell layers (Figure 3B and C) belong to amacrine or interplexiform “eremite” and “alloganglion” cells (Ehinger & Falck, 1969). We therefore do not know which, if any, TH cell somata are amacrine cells. We suppose that some might be, based on the shapes of previously described rodent dopaminergic amacrine cells (Voigt & Wässle, 1987; Zhang, Stone, Zhou, Ohta, & McMahon, 2004; Badea et al., 2009; Keeley & Reese, 2010). In the absence of means to distinguish large numbers of interplexiform and amacrine TH cells, we chose to pool our observations on neurites, considering those in the outer plexiform and inner nuclear layers as properties of interplexiform cells and those in the inner plexiform layer as characteristics of interplexiform and (if present) amacrine cells.

3.3 | Cell distributions and coverage factors

TH cell somata were observed at all eccentricities and in all sectors of flat-mounted whole retinae (e. g., Figure 4). When measured in square 1-mm^2 patches of retina (Figure 4A–D), TH cell densities varied from a maximum of 38/mm^2 in the middle of the superior-nasal quadrant to a minimum of 10 to 12/mm^2 at the retinal periphery (Figure 4E and F). Our TH cell counts fell within the ranges reported previously for adult rat and mouse (Savy et al., 1995; Nguyen-Legros, Versaux-Botteri, & Savy, 1997; Gustincich, Feigenspan, Wu,

Koopman, & Raviola, 1997; Zhang et al., 2004). In all of the flat-mounted whole retinae we examined ($n = 5$), the highest cell densities were found in the superior retina roughly midway between the optic disc and the retinal periphery (Figure 4E and F), and the lowest densities were found at the periphery of all quadrants. This formed an essentially radial, though offset, density gradient.

Previous studies have not reported coverage factors (Cleland et al., 1975) for rodent TH cells. We were able to trace the full length of the tapering neurites of some cells in our preparations (e. g., Figure 2B and I) and determine the area they covered (e. g., Figure 2C). Multiplying these areas by the density of TH cells within a 1-mm^2 square centered around each cell yielded a coverage factor of 1.86 ± 0.24 (mean ± *SEM*, $n = 17$; Figure 2). These coverage factors showed no dependence on cell density and ranged from 0.9 to 5.0 in all quadrants, at all eccentricities, and regardless of whether the soma was in the inner nuclear or ganglion cell layer (Figure 2F).

3.4 | Spines on TH cell somata, tapering neurites, and varicose neurites

Synaptic inputs to TH cells have been located by electron microscopy (Pourcho, 1982; Holmgren, 1982; Frederick et al., 1982; Hokoç & Mariani, 1987; Yazulla & Zucker, 1988; Pollard & Eldred, 1990; Kolb et al., 1990, 1991; van Haesendonck et al., 1993) and by pre- and postsynaptic protein localizations (Hoshi, Liu, Massey, & Mills, 2009; Dumitrescu, Pucci, Wong, & Berson, 2009; Contini et al., 2010). One study (Dacey, 1990) has proposed that bipolar cells synapse onto TH cells at appendages that resemble dendritic spines of other central neurons. Although bipolar cells are thought to drive dopamine input from retinal TH cells in general, spines have not been found on TH cells in the species studied here (Nguyen-Legros et al., 1981; Voigt & Wässle, 1987; Mitrofanis et al., 1988; Savy et al., 1995; Partida et al., 2004; Witkovsky et al., 2008; Fujieda & Sasaki, 2008; Debertin et al., 2015). Given that fine appendages on retinal ganglion cell dendrites are visible after fixation in sucrose-supplemented FA (Stradleigh et al., 2015), we examined TH cells for the presence of spines after fixation in sucrose-supplemented FA. After finding spines in raw confocally imaged optical sections, we used a PSF and a deconvolution algorithm to reverse or reassign blur and thus improve resolution in these sections (see Materials and Methods).

In agreement with results obtained in macaque (Dacey, 1990), we found spines on tapering neurites of rat TH cells (Figures 5A and C, 6D). In addition, we found spines on the somata and varicose neurites of TH cells (Figures 5B and D, and 6B and C). Notably, spines emerged from approximately half of the varicosities on TH cell neurites. (In a sample of 129 varicosities in the inner plexiform layer, 81 bore spines [e. g., Figures 5B, 6B, and 12]. In a sample of 131 varicosities in the outer plexiform layer, 66 bore spines [e. g., Figure 7].) By contrast, we found no spines on TH cell somata or neurites in retinae that were fixed in sucrose-free 4% FA (Figure 1A). As in other neurons (Jones & Powell, 1969; Peters & Kaiserman-Abramof, 1970), the spines of single TH cells varied in size and shape. In many cases, the diameter of the spine tip was either (a) larger than that of the neck portion (between the spine tip and the shaft of the parent neurite), (b) equal to the length of the neck, or (c) equal to the diameter and less than the length of the neck, as in “thin spines,” “stubby spines,” and “filopodia” of other preparations. Measured across z-stacks of deconvolved

images (cf. Arellano, Benavides-Piccione, Defelipe, & Yuste, 2007), the thin spines ranged in length from 0.4 to 2.9 μm (mean ± *SEM*: 1.2 ± 0.1 μm, $n = 57$), and displayed tips as large as 0.5 μm in diameter (mean ± *SEM*: 0.4 ± 0.01 μm, $n = 57$); stubby spines were generally shorter than 1 μm; and filopodia ranged in length from 0.6 to 10.1 μm (mean ± *SEM*: 1.6 ± 0.1 μm, $n = 105$). These properties did not noticeably differ between somata and neurites, between tapering and varicose neurites (Figures 5 and 6), or between Long–Evans and Lewis rats (Figures 5 and 6), and roughly half of the spines were thin spines in both strains. However, the spines of individual cells varied widely in their dimensions, and often did not show combinations of tip diameters, neck diameters, and lengths that split into distinct groups.

The sparsity of TH somata (especially in the ganglion cell layer), and of neurites in the outer plexiform layer and the proximal half of the inner plexiform layer, enabled us to image spines along somatic surfaces and neurite segments over distances exceeding 100 μm. These images showed spine densities of 2.6 ± 0.4, 2.3 ± 0.2, and 1.2 ± 0.1 (mean ± *SEM*) per 10 μm along the surface of somata ($n = 9$), inner plexiform layer neurites ($n = 42$), and outer plexiform layer neurites ($n = 18$), respectively. Whether similar densities are also found in s1 of the inner plexiform layer, both near to and far from individual somata, remains to be determined.

Spines were present on neighboring TH cells. Although this would be expected if all TH cells were spine-bearing, our results do not exclude the possibility that some TH cells lack spines. In fact, we were unable to find spines on some TH cells. This raises the possibility that both spine-bearing and spine-free TH cells exist in rat retina, as has been reported for TH cells in primate striatum and basal ganglia (Betarbet et al., 1997; Prensa, Cossette, & Parent, 2000). However, the most consistent difference we have found is that TH cells displayed more spines in some batches of Long–Evans rats than in other batches. To date, spine numbers in our preparations showed no consistent difference between rats of outbred (Long–Evans) and inbred (Lewis) strains, or between male and female rats; no clear dependence on the intensity of illumination that rats were exposed to prior to enucleation and during tissue processing; and no difference attributable to the temperature of solutions that retinae were immersed in during processing, or time of year.

3.5 | GluR1, GluR4, and NR1

Light-evoked intraretinal dopamine release, and the light response of at least some types of retinal TH cells, can be blocked by 2-amino-4-phosphonobutyric acid (APB) (Boatright, Gordon, & Iuvone, 1994a; Boelen et al., 1998; Zhang, Zhou, & McMahon, 2007; Zhang et al., 2008; Newkirk, Moon, Wong, & Detwiler, 2013). Because APB hyperpolarizes ON bipolar cells (Slaughter & Miller, 1981) and TH cell neurites arborize largely in s1 of the inner plexiform layer, one possible interpretation is that ON bipolar cells provide excitatory synaptic input to TH cells in the distal inner plexiform layer (Boelen et al., 1998). Immunostaining has shown pre- and postsynaptic protein appositions consistent with such inputs in rabbit (Hoshi et al., 2009; Dumitrescu et al., 2009; Contini et al., 2010), synapses from bipolar cells onto TH cells have been resolved by electron microscopy (Hokoç & Mariani, 1987, 1988; Kolb et al., 1990), and amperometry has shown that glutamate receptor

agonist applications can release dopamine from dissociated mouse TH cells (Puopolo et al., 2001). Based on these findings, and the binding of antibodies directed against glutamate receptor subtypes in the inner nuclear and inner plexiform layers (Peng, Blackstone, Huganir, & Yau, 1995; Qin & Pourcho, 1996; Grünert, Haverkamp, Fletcher, & Wässle, 2002; Jakobs, Ben, & Masland, 2003; Hoshi et al., 2009; Contini et al., 2010), we tested whether antibodies directed against GluR1 and GluR4 bind to TH cells in our preparations. In agreement with previous studies, we found clear and reproducible staining by anti-glutamate receptor antibodies in whole-mounted retinae after immersion in fixative for 20 min (Hartveit et al., 1994; Gründer et al., 2000), but not if the fixation period was 1 hr or longer (Morigiwa & Vardi, 1999; Witkovsky et al., 2008).

GluR1-immunopositive pixel clusters (referred to hereafter as “GluR1”) were found on TH cell somata (Figure 8), tapering neurites (not illustrated), and varicose neurites (Figures 7 and 12), on spines (Figure 8), and along the shafts of neurites (Figures 7 and 12). GluR1 colocalized with TH, as would be expected if TH cells expressed GluR1, in all of the retinal layers where TH was found, viz., the outer plexiform (Figure 7), inner nuclear (not illustrated), inner plexiform (Figure 12), and ganglion cell (Figure 8) layers. An average of 9.1 ± 2.3 (mean ± *SEM*; range: 3–18) colocalizations of GluR1 and TH were found per cell ($n = 7$) on the somata and the portions of the neurites of cells that could be distinguished from processes of other cells. The numbers of colocalizations per 10 μm of membrane along the surface of these somata were similar to those along the lengths of neurites (0.52 ± 0.11 and 0.63 ± 0.07, respectively).

Previous studies have tested whether GluR1 colocalizes with TH by chance (Contini et al., 2010; see also Dumitrescu et al., 2009). For comparison, we performed a Monte Carlo permutation analysis on four cells. Based on 10,000 repeats per cell (see Materials and Methods for details), we found that the observed GluR1 spots were more likely to be located within 0.2 μm of each TH cell than GluR1 spots whose locations in xyz space were generated by randomly mixing the xyz coordinate values of the observed spots. The count of observed (O_c) and randomly generated (R_c, mean ± standard deviation [*SD*]) spots within that distance were 331 and 133.9 ± 11.2, 926 and 861.7 ± 23.9, 513 and 421.1 ± 17.8, and 3050 and 2970.9 ± 43.9 for these cells. The probability that R_c exceeded or was equal to O_c was less than 10e-5, equal to 0.0027, less than 10e-5, and equal to 0.0376, respectively. Because these p values are all below 0.05, we interpret them as rejecting the null hypothesis that the observed TH/GluR1 colocalization occurred by chance. Although the difference between O_c and R_c values is larger than the number of GluR1 and TH colocalizations noted above, this is consistent with inclusion (in O_c) of GluR1 spots that fluoresced too dimly to meet the criterion for colocalization by eye (viz., summing to white when the GluR1 and TH were displayed in magenta and green color channels, respectively).

GluR1 was also found in between TH cell surfaces in the inner plexiform layer (Figures 8 and 12A). This staining is consistent with previous findings that anti-GluR1 antibodies bind to other cell types in the inner retina, including ganglion cells and non-TH amacrine cells (Gründer et al., 2000; Grünert et al., 2002; Lin, Martin, & Grünert, 2002). Side views (Figure 12B–E) of the field in Figure 12A show that the GluR1 immunostaining intensity in the inner plexiform layer exceeds that in the adjacent inner nuclear and ganglion cell layers.

Similar staining patterns were observed with anti-GluR1 and anti- GluR4 antibodies. This was not surprising given that they have been found to bind to retinal TH cells in other species (Hoshi et al., 2009; Contini et al., 2010). Thus, anti-GluR4 antibody binding was found on rat TH cell neuritic (Figure 9) and somatic (not illustrated) spines (on $n = 3$ cells).

It is not known whether the glutamate receptor agonist NMDA can increase retinal dopamine release. However, glutamate can activate NMDA receptors in midbrain TH cells (Overton & Clark, 1992), NMDA receptors colocalize with α-amino-3-hydroxy-5-methyl-4-isoxazolepropionate (AMPA) receptors in midbrain TH cells (Chatha, Bernard, Streit, & Bolam, 2000), and antibodies directed against the NR1 subunit of NMDA receptors bind in the proximal inner nuclear layer and the inner plexiform layer (Fletcher et al., 2000; Zhang & Diamond, 2006). As seen with anti-GluR1 and anti-GluR4 antibodies, anti-NR1 antibodies bound to neuritic spines (on $n = 3$ cells), either at their tips or along their necks (e. g., panel 1d of Figure 10). As many as seven GluR1, five GluR4, and seven NR1 pixel clusters were found on segments of single TH cell neurites captured within imaged fields.

The average spatial density of these clusters in neurites, pooled with the densities in somata, was 0.6 ± 0.1 colocalizations of GluR1 and TH ($n = 10$), 0.7 ± 0.1 colocalizations of GluR4 and TH ($n = 5$), and 0.6 ± 0.1 colocalizations of NR1 and TH ($n = 10$), per 10 μm of neurite segment or of somatic membrane (mean ± *SEM*; range: 0.3–1.2). These densities did not significantly differ with the total number of colocalizations per structure (range 2–7).

We did not test for the presence of other glutamate receptor isoforms. For example, although anti-GluR2/3 antibodies have been found to bind to rat retinal TH cells (Gábriel, de Souza, Ziff, & Witkovsky, 2002), the binding is cytoplasmic and thus not in subcellular regions of interest for this study. In addition, although GluR2/3 immunoreactivity is found in processes postsynaptic to most bipolar cell ribbon synapses, GluR4 is found at a similar, if not larger, fraction of these synapses (Qin & Pourcho, 1999; Grünert et al., 2002).

3.6 | $GABA_A$

In addition to glutamate, GABA receptor ligands can alter dopamine release, with agonists (GABA and muscimol) inhibiting light-evoked dopamine release (Kirsch & Wagner, 1989; Boatright, Rubim, & Iuvone, 1994b) and antagonists (bicuculline and picrotoxin) stimulating intraretinal dopamine release (O'Connor, Dorison, Watling, & Dowling, 1986; Kirsch & Wagner, 1989), and GABA inhibiting spontaneous dopamine release from dissociated TH cells (Puopolo et al., 2001). Based on these findings and the detection of $GABA_A$ receptor subunits and mRNA in inner nuclear layer somata of rat and mouse retinae (Brecha, Sternini, & Humphrey, 1991; Greferath et al., 1995; Newkirk et al., 2013), we tested whether an antibody directed against $GABA_AR_{\alpha 1}$ binds to TH cells. Images of double-labeled preparations (Figure 11) show that this anti-$GABA_AR_{\alpha 1}$ antibody binds to spots along the surface of TH cell somata and neurites. However, the distribution of this binding differed in two respects from that of the anti-glutamate receptor antibodies listed above. First, anti-$GABA_AR_{\alpha 1}$ antibodies did not stain the tip or neck of any types of spines. Second, the immunopositive spots appeared to be widely and evenly distributed over TH cell somata and tapering neurites, forming an outline of the TH cell when the TH cell color channel was turned off (e. g., Figure 11B).

3.7 | PSD-95, PSD-93, and RIBEYE

We tested the possibility that GluR1-, GluR4-, and NR1-immunopositive foci are sites of synaptic input in two ways. First, we probed preparations for combinations of postsynaptic markers by triple labeling for TH, the glutamate receptor isoforms examined above (GluR1, GluR4, NR1), and the PSD proteins PSD-95 and PSD-93. The latter were selected because postsynaptic submembrane densifications are found in TH cells at synapses from bipolar cells (Hokoç & Mariani, 1987; Contini et al., 2010), at least some cells receiving glutamatergic inputs express PSD-95 and PSD-93 (Sheng & Kim, 2011), and PSD-95 and PSD-93 are found at multiple levels of the inner plexiform layer (Koulen, Fletcher, Craven, Bredt, & Wässle, 1998). Although we did not probe for all known glutamate receptors and PSD proteins, the combinations we tested did show that PSD proteins colocalize at some points on the surface of TH cells with glutamate receptor proteins. Specifically, PSD-95 colocalized at some points on the surface of TH cells with GluR1 (Figure 8) and GluR4 (Figure 9), and PSD-93 colocalized at some points on the surface of TH cells with NR1 (Figure 10). Some of these colocalizations were found on somatic and neuritic spines (panel 4c of Figure 8; panels 1d and 2d of Figure 9; and panel 1d′ of Figure 10), whereas others were found on the shafts of neurites (Figure 7). In addition to these, several foci of PSD-95 and PSD-93 were found in TH cells without GluR1, GluR4, or NR1 immunoreactivity, and vice versa (panels 1c, 2c, and 3c of Figure 8; panel 3d of Figure 9; and panels 2d′ and 3d′ of Figure 10).

Second, we probed preparations for combinations of pre- and postsynaptic markers by triple labeling for TH, RIBEYE (Schmitz, Königstorfer, & Südhof, 2000), and GluR1. This approach was similar to that used to locate bipolar cell inputs to rabbit TH cells (Hoshi et al., 2009), except that we used sucrose-supplemented FA to preserve the neurites and spines of TH cells, and we did not use anti-calbindin antibodies to label bipolar cells because they stain horizontal cells instead of bipolar cells in rat (Röhrenbeck, Wässle, & Heizmann, 1987). Single optical sections showed RIBEYE apposed to colocalizations of TH and GluR1 in the inner plexiform layer (Figure 12), resembling the arrangements of TH, RIBEYE, and GluR4 in rabbit TH cells (Hoshi et al., 2009).

4 | DISCUSSION

This study has re-examined the morphology and immunostaining of retinal TH cells. The TH cells in our preparations differ from all previously described TH cells in that the somata, tapering neurites in the inner plexiform layer, and varicose neurites in the inner and outer plexiform layers, bear spines. Other studies have noted the presence of similar spines in TH cells, but these were found exclusively on either tapering dendrites (Dacey, 1990) or varicose neurites (Teakle et al., 1984) in the inner plexiform layer, or as short processes on the distal side of TH cell somata (Pollard & Eldred, 1990; Gábriel et al., 1991). We also found, for the first time, glutamate receptor-, PSD-95-, and PSD-93-immunopositive spines on retinal TH cell somata and neurites, and GABA receptor-immunopositive foci on rat TH cell somata and neurites. These results are discussed below, particularly with regard to 4% FA as a fixative, the normal morphology of TH cells, and the modulation of dopamine release by glutamate and GABA.

4.1 | Aldehyde fixation

Our results show that TH cell neurites appear to be segmented, and that TH cell somata and neurites appear to be spine-free, in adult rat retinae immersed in 4% FA immediately after dissection (Figure 1). Similar degrees of segmentation were found in previous TH cell studies of some species (e. g., Versaux-Botteri, Nguyen-Legros, Vigny, & Raoux, 1984; Mitrofanis & Provis, 1990), but not others (Oyster et al., 1985; Voigt & Wässle, 1987). The neurite segmentation and spine loss we have found in rat TH cells after immersion in 4% FA constitute different, and more severe, damage than the beading and shrinkage of interbead segments we previously found in rat retinal ganglion cell dendrites and axons exposed to the same fixative (Stradleigh et al., 2015).

We have not identified cellular changes that lead to neurite segmentation or spine loss following immersion in 4% FA. Instead, we focused on the morphological properties that better preservation reveals in sucrose-supplemented FA. For example, the spread and overall shape of tapering and varicose neurites of cells fixed in sucrose-supplemented FA resembled the dendrites and axons of dye-injected and marker-expressing TH cells of other species (Dacey, 1990; Zhang et al., 2004; Badea et al., 2009; see also Voigt & Wässle, 1987; Tauchi et al., 1990; Newkirk et al., 2013) and the neurites of TH cells in other immunostained preparations (e. g., Oyster et al., 1985; Kolb et al., 1990; Teakle et al., 1993). In addition, given their presence in retinae incubated in an aldehyde fixative that protects retinal ganglion cells from artifactual formation of varicosities (Stradleigh et al., 2015), we infer that somatic and neuritic spines are normal traits of rat TH cells. Moreover, we found that relatively brief (20-min) immersions in sucrose-supplemented FA preserves TH cell structural features (including neurite shape, contour, and spines) and enabled us to detect anti-glutamate receptor antibody binding to TH cells.

Previous studies have shown that other fixatives can also preserve TH cell spines, including 4% formaldehyde and 1% glutaraldehyde (Dacey, 1990); 2% to 5% glutaraldehyde (Mariani, 1990); and 2% formaldehyde, L-lysine, and sodium metaperiodate (Teakle et al., 1994). The presence of spines on TH cells in macaque retinae fixed in formaldehyde and glutaraldehyde (see Figure 4 of Dacey, 1990) but not in macaque retinae fixed in 4% FA (see Figure 11 of Dacey, 1990) agrees with our finding that rat TH cells possess and lack spines in retinae fixed in sucrose-supplemented and straight 4% FA, respectively.

4.2 | Cell distribution and coverage factor

Previously reported TH cell densities range from 10 to 40/mm^2 (Mariani, Kolb, & Nelson, 1984; Voigt & Wässle, 1987; Tauchi et al., 1990; Dacey, 1990; Gustincich et al., 1997; Ngyuen-Legros et al., 1997), although higher values (~60/mm^2) have been found around the foveal pits of macaque and *Cebus* (Dacey, 1990; Guimarães & Hokoç, 1997) and in the visual streak of turtle (Kolb, Cline, Wang, & Brecha, 1987). The radial gradient of TH cell densities we found (Figure 4) is similar to that shown in a previous description of rat retina (Nguyen-Legros et al., 1997) and differs from a reported monotonic density decline from the superior-temporal quadrant to the inferior-nasal quadrant (Mitrofanis et al., 1988), the uniform distribution of horizontal cells (Peichl & Gonzalez-Soriano, 1994), and the paired high-density regions of rod bipolar cells (Euler & Wässle, 1995). The radial gradient

resembles the gradient of AII amacrine cells in rat retina (Wässle, Grünert, & Röhrenbeck, 1993), as might be expected given that AII amacrine cells are a major target of TH cell output synapses (Pourcho, 1982; Voigt & Wässle, 1987).

TH cell densities and dendritic field dimensions are known for at least one species of all vertebrate classes (goldfish: van Haesendonck et al., 1993; toad: Zhu & Straznicky, 1990; turtle: Kolb, Netzer, & Ammermüller, 1997; chick: Teakle et al., 1993; cat: Voigt & Wässle, 1987; macaque: Dacey, 1990). The products of these range from 1.1 (Teakle et al., 1993) to 4.8 (Schütte & Witkovsky, 1991), with intermediate values of 3.4 and 1.9 to 3.8 reported for cat and macaque, respectively (Voigt & Wässle, 1987; Dacey, 1990). The product of the cell densities and the fields of tapering neurites we found are smaller than the largest values reported for other species, but by less than two-fold. The extent to which this describes the coverage of visual space by TH cells remains to be seen. If, as our data suggest, excitatory synaptic inputs are formed on varicose as well as tapering neurites, the coverage factors of TH cells are likely to be substantially larger than values estimated only from tapering neurites. Although this would be best addressed by formation of a connectome (e. g., Anderson et al., 2009), reconstructing and mapping bipolar cell inputs at high resolution along neurites that extend millimeters across the retina (Dacey, 1990; Badea et al., 2009) were beyond the scope of the present study. In vivo imaging of cells that are induced to express, or are filled by, a brightly fluorescent marker (cf. Voigt & Wässle, 1987; Tauchi et al., 1990; Dacey, 1990; Badea et al., 2009; Keeley & Reese, 2010; Zhang et al., 2004) might also be attempted. However, it is unlikely that the methods available can resolve the spines we have studied here and, at the same time, image neurites that arborize across most, or all, of the retinal surface (cf. Geng et al., 2011).

4.3 | TH cell neurites and spines

Two kinds of neurites are referred to as axons in the retina—those carrying signals toward the optic nerve from rod, cone, bipolar, and ganglion cell somata, and those carrying signals at some distance from the somata and dendrites of horizontally arborizing interneurons. How this applies to mammalian TH cells is not clear for at least three reasons. First, it is not known whether the neurites that extend away from TH cell somata are functionally polarized by spatially differential distributions of their input and output synapses. Notably, some varicose neurites emerge from tapering neurites, but others emerge from somata and are thus less likely to be depolarized by signals propagating centrifugally from tapering neurites. Second, it is not known whether signals propagate radially through their neuritic arbors (Taylor, 1996; Davenport et al., 2007) or whether varicose regions of TH cell neurites hinder signal spread over long distances (Ellias & Stevens, 1980). Third, previous studies have denoted neurites of different shapes as dendrites and, in addition, neurites of different shapes as axons. For example, some studies have referred to TH cell neurites as dendrites if they are a few μm in diameter where they emerge from somata, gradually taper, branch more than once, and are studded with spines, and as axons (or axon-like) if they originate from a soma or a dendrite close to a soma, immediately taper to a thin (~0.5-μm) process, bear varicosities, branch sparsely, and radiate beyond the dendritic tree (e. g., Dacey, 1990; Badea et al., 2009). Other studies have reported that TH cell dendrites are varicose (Kolb et al., 1990; Dann, 1998; Zhang et al., 2004), that TH cell axons have few or no varicosities

(Guimarães & Hokoç, 1997; Witkovsky et al., 2005), and that TH cell dendrites ramify in s1 and that axons (or axon-like neurites) ramify in s3 and s5 (Gábriel et al., 1992; Debertin et al., 2015). Still other studies have described TH cell dendrites and not axons (e. g., Voigt & Wässle, 1987; Tauchi et al., 1990). It is not known whether these TH cell neurites differ functionally as much as they appear to differ anatomically.

Our results indicate that tapering and varicose neurites do not differ dichotomously, in that both bind antibodies directed against glutamate receptor and PSD proteins (Figures 7, 9, and 12). Moreover, because spines on tapering and varicose neurites both bound these antibodies (e. g., panel 1d of Figure 10 and panel 1d of Figure 12), and because glutamate receptors and PSD proteins are commonly found at glutamatergic synapses (Sheng & Kim, 2011), our results suggest that spines on tapering and varicose neurites are sites of at least some glutamatergic input to TH cells. Although spines are most well known as dendritic specializations, spines are also found on axons (e. g., Westrum, 1970). We therefore chose to denote tapering and varicose processes of rat TH cells as neurites rather than dendrites and axons. Future imaging and/or electrophysiological studies could test whether excitatory synapses onto tapering neurites drive dopamine release from varicose neurites (Dacey, 1990; Witkovsky et al., 2008) or, alternatively, whether varicose neurites are depolarized by excitatory synapses onto the varicose segments themselves.

Cerebellar Purkinje cells, and pyramidal cells in hippocampus and cerebral cortex, display spine densities as high as 150 spines per 10 μm. The spine densities in TH cells we have found to date are nearly 100-fold lower. However, our counts agree well with spine densities of substantia nigra TH cells (Jang et al., 2015; Hage, Sun, & Khaliq, 2016), cortical “sparsely spinous” neurons (Feldman & Peters, 1978), and neostriatal type II neurons (Graveland, Williams, & DiFiglia, 1985), and also with the uncounted but seemingly similar spine densities in previous retinal TH cell studies (Teakle et al., 1984; Dacey, 1990). At least some of these spines may be positioned to depolarize dopamine release sites locally, for example, in cases where they are positioned at varicosities (e. g., panels 1a–d of Figure 12; also, see below). It will be of interest to test whether this applies to all TH cell spines, because the spine densities we have found to date (1–3 per 10 μm) exceed the density of sites that bind antibodies directed against combinations of glutamate receptor isoforms and presynaptic markers in rabbit TH cells (see Figure 2a of Hoshi et al., 2009) and are comparable to those in mouse TH cells (see Figure 7A of Contini et al., 2010).

4.4 | Synaptic inputs to TH cell somata and neurites

The immunostainings found in this study are consistent with synaptic inputs to TH cells that include previously undescribed and previously reported types. The former include glutamatergic inputs to spines on TH cell somata, spines on TH cell neurites in the inner plexiform layer, and TH cell spines in the outer plexiform layer. The latter include glutamatergic inputs to shafts of TH cell neurites and GABA-ergic inputs to TH cell somata.

As found previously in some nonretinal neuronal somata (Jaffe, Marty, Schulte, & Chow, 1998), rodent TH cell somata can release dopamine (Puopolo et al., 2001). Glutamate and kainate can augment this release (Puopolo et al., 2001), and our finding GluR1 (and, in some cases, both GluR1 and PSD-95) on TH cell somatic surfaces and spines suggests that these

glutamate and kainate effects might normally be mediated at spines and at membrane patches between spines. Although the cells eliciting these effects remain to be identified in rat retina, bipolar cells are the most likely candidates given that their axons project from the inner nuclear layer to the ganglion cell layer, and form glutamatergic synapses. Consistent with this possibility, the synaptic ribbon protein RIBEYE has been found in ON bipolar cell axons where they appose TH cell somata in the rabbit retina inner nuclear layer (Hoshi et al., 2009), and rat retinal bipolar cell axons have been found to bind antibodies directed against synaptic vesicle-associated proteins in the proximal half of the inner nuclear layer (Sherry, Wang, Bates, & Frishman, 2003) where most rat TH cell somata reside. Similarly, the axons of at least two types of bipolar cell (rod and CB9-type cone bipolar cells) extend into the ganglion cell layer (Euler & Wässle, 1995; Hartveit, 1997; Østergaard, Hannibal, & Fahrenkrug, 2007; Grünert, Jusuf, Lee, & Nguyen, 2011) where alloganglion TH cell somata reside, and a synaptic ribbon protein (piccolo) can be found as far proximally as the ganglion cell layer (Grünert et al., 2011).

In the inner plexiform layer, we found three immunostaining patterns that are consistent with glutamatergic inputs to TH cell neurites: apposition of RIBEYE to colocalizations of GluR1 and TH (Figure 12), colocalizations of GluR4 and PSD-95 (Figure 9), and colocalizations of NR1 and PSD-93 (Figure 10). The GluR4 and NR1 we have found on tapering TH cell neurites (Figures 9 and 10) are consistent with the hypothesis that bipolar cell inputs depolarize TH cell dendrites (Dacey, 1990). At the same time, our finding GluR1 and NR1 on varicose neurites of TH cells is not consistent with the hypothesis that varicose neurites are solely presynaptic compartments (Dacey, 1990) and suggests, instead, that varicose neurites may be postsynaptic as well as presynaptic. Specifically, our images suggest that postsynaptic membrane might be located on a varicosity (panels 2a–d of Figure 12), on a neuritic shaft that is adjacent to a varicosity (panels 2a–c of Figure 7), or on a spine that is adjacent to, or emerges from, a varicosity (panels 1a–d′ of Figure 10).

In the outer plexiform layer, we found two immunostaining patterns that are consistent with glutamatergic inputs to TH cell neurites: colocalizations of GluR1 and TH on spines (panel 1c of Figure 7) and shafts of neurites (panel 2c of Figure 7). The spines we have found on at least half of the varicosities in TH cell neurites within the outer plexiform layer (Figure 7B) may also be driven by glutamatergic inputs (cf. panel 1a of Figure 7 and panel 1a of Figure 10). This would be of interest, because glutamatergic synapses on varicosities and/or on spines attached to the varicosities could depolarize varicose neurites either in addition to spikes that propagate along voltage-gated Na^+ channel-expressing internal neurites (Witkovsky et al., 2004), or independently of spikes in external neurites given their lack of voltage-gated Na^+ channels (Witkovsky et al., 2008), and these depolarizations could drive the synapses that TH cell external neurites form onto horizontal cells and possibly other interneurons (Dowling & Ehinger, 1975; Kolb et al., 1990). Although the source of the glutamatergic inputs to TH cells at the outer plexiform layer remains to be identified, a previous study suggested that glutamate can diffuse from cone ribbon synapses to glutamate receptors several μm beneath cone pedicles in the macaque outer plexiform layer (Haverkamp et al., 2000), and bipolar cells have previously been found to form synapses onto cells beside horizontal cells in the salamander outer plexiform layer (Lasansky, 1980).

To date, we have encountered only small numbers of triple labelings on individual cells. However, the most closely spaced of these were separated by ~20 μm (range: 3–44 μm), comparable to the estimated density of bipolar cell ribbon synapses onto mouse TH cell dendrites (Dumitrescu et al., 2009). Notably, GluR1, GluR4, and NR1 colocalized with TH more often than this at sites not showing detectable levels of PSD-95 or PSD-93. In addition, we did not find GluR1, GluR4, or NR1 on several spines in our preparations. It remains to be seen whether these spines express these isoforms at levels that we could not detect, express these isoforms under conditions that we did not test (e. g., complete darkness), or express other glutamate receptor isoforms. Also, it is unknown which glutamate receptors are present at individual synapses on TH cells, and thus do not yet know if the different colocalizations we have found reflect different postsynaptic sites.

The presence of $GABA_AR_{\alpha 1}$ on TH cell somata in our preparations agrees with electron microscopic observations that GABA-immunopositive cells form synapses onto TH cell somata (Kolb et al., 1991). Likewise, the heavy investment of $GABA_AR_{\alpha 1}$ around TH cell neurites is consistent with the electron microscopic observations that amacrine cells form synapses onto TH cell processes in the inner plexiform layer (Dowling & Ehinger, 1975; Hokoç & Mariani, 1987, 1988; Kolb et al., 1990). Although the source of the GABAergic inputs to the base of TH cell somata and to the neurites (especially in s1) might be GABAergic amacrine cells, amacrine cells do not arborize in the inner nuclear layer where we find conspicuous staining, for example, at the levels of distal and lateral sides of the TH cell somata, and along TH-immunopositive neurites traversing the inner nuclear layer. GABAergic interplexiform cells (Nakamura et al., 1980) are a possible source of inputs to these TH cell compartments, given that their neurites traverse the inner nuclear layer. Moreover, precedents for synapses like this are provided by interplexiform cell synapses onto amacrine cell somata (Linberg & Fisher, 1986; Yazulla & Studholme, 1991).

4.5 | Double versus triple labeling

Given that both AMPA and NMDA receptor proteins have been found at synapses on other neurons (Siegel et al., 1995; Petralia et al., 1999), and that PSD-95 forms postsynaptic complexes with AMPA and NMDA receptors (Kornau, Schenker, Kennedy, & Seeburg, 1995; Vinade et al., 2003), our results raise two questions. One is why some GluR1 and GluR4 pixel clusters colocalized with detectable levels of PSD-95 and some did not. The second is why some PSD-95 pixel clusters were detectable in TH cells, yet did not appear to colocalize with GluR1 or GluR4.

Possible answers to the first question are that other PSD proteins substitute for PSD-95 at these sites or, alternatively, that synaptic transmission can occur in the absence of PSD proteins. Dopaminergic substantia nigra neuron dendrites have been reported to lack PSD-95 (Inanobe et al., 1999) and PSD proteins other than PSD-95 have been detected in the proximal retina (Fletcher et al., 2000; Ghosh, Haverkamp, & Wässle, 2001; Brandstätter, Dick, & Boeckers, 2004). On the other hand, glutamate receptors can be activated before formation of detectable PSDs, at least at some spines (de Roo, Klauser, Mendez, Poglia, & Muller, 2008), PSD size correlates inversely with head volume in some spines (Cane, Maco, Knott, & Holtmaat, 2014), and PSD-95 can have half-lives that are shorter than those of

spines and synapses (Gray, Weimer, Bureau, & Svoboda, 2006). Possible answers to the second question are that GluR1 and/or GluR4 were present at levels that our imaging methods did not detect, that PSD-95 and PSD-93 associate with receptor isoforms other than GluR1 or GluR4, or that GluR1 and GluR4 were internalized by TH cells under our experimental conditions. Although PSDs have been found to increase with spine head size (Harris & Stevens, 1989), our finding (Figure 10) PSD-93 at the tip of spines with no detectable head (i. e., filopodia) near immunonegative spines with heads of moderate size (i. e., thin spines) indicates that the paucity of glutamate receptor staining of spines in our preparations is not necessarily due to small head size. It is difficult to predict which glutamate receptors might be expressed by TH cells because some studies have found that TH cells bind anti-GluR1 and anti-GluR4 antibodies (Figures 7–9, and 12) (Hoshi et al., 2009; Contini et al., 2010) whereas other studies did not (Witkovsky et al., 2008). Previous findings that synaptic activity can lead to glutamate receptor removal from synapses (O'Brien et al., 1998; Carroll, Lissin, von Zastrow, Nicoll, & Malenka, 1999) are of particular interest, given that glutamatergic synapses are thought to drive dopamine release from TH cells and that light can drive this release for several hours per day (Megaw, Boelen, Morgan, & Boelen, 2001). Future studies could test whether TH cell synapses and spines are altered morphologically and functionally by changes in illumination.

5 | CONCLUSIONS

Two general observations emerge from this study. One is that retinal TH cells are endowed with both somatic and neuritic spines. Although our results suggest that some of these may enable glutamate to control dopamine release from TH cells, many of the spines we observed were not labeled by the antibodies we tested. Future studies could test the possibility that spatially restricted glutamate applications can activate receptors in these spines (Matsuzaki et al., 2001) or that these spines respond to other inputs (Hare & Owen, 1995; Kouvidi, Papadopoulou-Daifoti, & Thermos, 2005; Zhang et al., 2008; Vuong, Hardi, Barnes, & Brecha, 2015). The second is that synapses on TH cell somatic spines, together with other synapses found in the inner nuclear layer (e. g., Fisher, 1972; Dowling & Ehinger, 1975; Marc & Liu, 1984; Sakai & Naka, 1985; Linberg & Fisher, 1986; Zucker & Dowling, 1987), support the notions that the inner nuclear and ganglion cell layers are more than layers of somata, and that retinal synapses are not formed exclusively within the inner and outer plexiform layers. Future studies could test whether TH cells that respond to light differently (Zhang et al., 2007) comprise one or more morphological subtypes (cf. Jones, Marc, & Watt, 2004; Newkirk et al., 2013), whether individual TH cells are excited directly by bipolar cell input and simultaneously by decreases in inhibitory input, or whether some subtypes of TH cells are driven by excitatory bipolar cell input and others are driven by release from inhibition by amacrine and interplexiform cells.

Acknowledgments

The authors thank K. Zito and G.J. Partida for discussions and comments on the manuscript, M.R. Paddy and F.F. Ventimiglia for discussions and advice on deconvolution, I. Brust-Mascher for advice on deconvolution and image analysis, and T.W. Stradleigh for observations at the beginning of this study, advice on immunohistochemistry, and comments on the manuscript.

Funding information

National Institutes of Health, Grant/Award Numbers: EY008120 (to A.T.I.) and P30 EY012576 (to J.S. Werner); Research to Prevent Blindness (to the Department of Ophthalmology, U.C. Davis).

References

Anderson JR, Jones BW, Yang JH, Shaw MV, Watt CB, Koshevoy P, Marc RE. A computational framework for ultrastructural mapping of neural circuitry. PLoS Biology. 2009; 7(3):e1000074. [PubMed: 19855814]

Arellano JI, Benavides-Piccione R, Defelipe J, Yuste R. Ultrastructure of dendritic spines: Correlation between synaptic and spine morphologies. Frontiers in Neuroscience. 2007; 1:131–143. [PubMed: 18982124]

Badea TC, Hua ZL, Smallwood PM, Williams J, Rotolo T, Ye X, Nathans J. New mouse lines for the analysis of neuronal morphology using CreER(T)/loxP-directed sparse labeling. PLoS One. 2009; 4:e7859. [PubMed: 19924248]

Betarbet R, Turner R, Chockkan V, DeLong MR, Allers KA, Walters J, Greenamyre JT. Dopaminergic neurons intrinsic to the primate striatum. Journal of Neuroscience. 1997; 17:6761–6768. [PubMed: 9254687]

Boatright JH, Gordon JR, Iuvone PM. Inhibition of endogenous dopamine release in amphibian retina by L-2-amino-4-phosphonobutyric acid (L-AP4) and trans-2-aminocyclopentane-1,3-dicarboxylate (ACPD). Brain Research. 1994a; 649:339–342. [PubMed: 7525012]

Boatright JH, Rubim NM, Iuvone PM. Regulation of endogenous dopamine release in amphibian retina by gamma-aminobutyric acid and glycine. Visual Neurocience. 1994b; 11:1003–1012.

Boelen MK, Boelen MG, Marshak DW. Light-stimulated release of dopamine from the primate retina is blocked by 1–2-amino-4-phosphonobutyric acid (APB). Visual Neurocience. 1998; 15:97–103.

Brainard GC, Morgan WW. Light-induced stimulation of retinal dopamine: A dose-response relationship. Brain Research. 1987; 424:199–203. [PubMed: 3690300]

Brandstätter JH, Dick O, Boeckers TM. The postsynaptic scaffold proteins ProSAP1/Shank2 and Homer1 are associated with glutamate receptor complexes at rat retinal synapses. The Journal of Comparative Neurology. 2004; 475:551–563. [PubMed: 15236236]

Brecha NC, Sternini C, Humphrey MF. Cellular distribution of L-glutamate decarboxylase (GAD) and gamma-aminobutyric acidA (GABAA) receptor mRNAs in the retina. Cellular and Molecular Neurobiology. 1991; 11:497–509. [PubMed: 1660350]

Cane M, Maco B, Knott G, Holtmaat A. The relationship between PSD-95 clustering and spine stability in vivo. Journal of Neuroscience. 2014; 34:2075–2086. [PubMed: 24501349]

Carroll RC, Lissin DV, von Zastrow M, Nicoll RA, Malenka RC. Rapid redistribution of glutamate receptors contributes to long-term depression in hippocampal cultures. Nature Neuroscience. 1999; 2:454–460. [PubMed: 10321250]

Chatha BT, Bernard V, Streit P, Bolam JP. Synaptic localization of ionotropic glutamate receptors in the rat substantia nigra. Neuroscience. 2000; 101:1037–1051. [PubMed: 11113353]

Chen YC, Chiao CC. Symmetric synaptic patterns between starburst amacrine cells and direction selective ganglion cells in the rabbit retina. The Journal of Comparative Neurology. 2008; 508:175–183. [PubMed: 18306383]

Cleland BG, Levick WR, Wässle H. Physiological identification of a morphological class of cat retinal ganglion cells. Journal of Physiology. 1975; 248:151–171. [PubMed: 1151804]

Contini M, Raviola E. GABAergic synapses made by a retinal dopaminergic neuron. Proceeding of the National Academy of Science of the United State of America. 2003; 100:1358–13563.

Contini M, Lin B, Kobayashi K, Okano H, Masland RH, Raviola E. Synaptic input of ON-bipolar cells onto the dopaminergic neurons of the mouse retina. The Journal of Comparative Neurology. 2010; 518:2035–2050. [PubMed: 20394057]

Crooks J, Kolb H. Localization of GABA, glycine, glutamate and tyrosine hydroxylase in the human retina. The Journal of Comparative Neurology. 1992; 315:287–302. [PubMed: 1346792]

Dacey DM. The dopaminergic amacrine cell. The Journal of Comparative Neurology. 1990; 301:461–489. [PubMed: 1979792]

Dann JF. Dopaminergic amacrine cells in the retina of the possum, Trichosurus vulpecula. Visual Neurocience. 1998; 15:701–709.

Davenport CM, Detwiler PB, Dacey DM. Functional polarity of dendrites and axons of primate A1 amacrine cells. Visual Neurocience. 2007; 24:449–457.

Debertin G, Kántor O, Kovács-Öller T, Balogh L, Szabó-Meleg E, Orbán J, Völgyi B. Tyrosine hydroxylase positive perisomatic rings are formed around various amacrine cell types in the mammalian retina. Journal of Neurochemistry. 2015; 134:416–428. [PubMed: 25940543]

de Roo M, Klauser P, Mendez P, Poglia L, Muller D. Activity-dependent PSD formation and stabilization of newly formed spines in hippocampal slice cultures. Cerebral Cortex. 2008; 18:151–161. [PubMed: 17517683]

Dowling JE, Ehinger B. Synaptic organization of the amine-containing interplexiform cells of the goldfish and Cebus monkey retinas. Science. 1975; 188:270–273. [PubMed: 804181]

Dumitrescu ON, Pucci FG, Wong KY, Berson DM. Ectopic retinal ON bipolar cell synapses in the OFF inner plexiform layer: Contacts with dopaminergic amacrine cells and melanopsin ganglion cells. The Journal of Comparative Neurology. 2009; 517:226–244. [PubMed: 19731338]

Eglen SJ, Raven MA, Tamrazian E, Reese BE. Dopaminergic amacrine cells in the inner nuclear layer and ganglion cell layer comprise a single functional retinal mosaic. The Journal of Comparative Neurology. 2003; 466:343–355. [PubMed: 14556292]

Ehinger B, Falck B. Adrenergic retinal neurons of some new world monkeys. Zeitschrift fur Zellforschung und Mikroskopische Anatatomie. 1969; 100(3):364–75.

Ellias SA, Stevens JK. The dendritic varicosity: A mechanism for electrically isolating the dendrites of cat retinal amacrine cells? Brain Research. 1980; 196:365–372. [PubMed: 6249448]

Euler T, Wässle H. Immunocytochemical identification of cone bipolar cells in the rat retina. The Journal of Comparative Neurology. 1995; 361:461–478. [PubMed: 8550893]

Euler T, Detwiler PB, Denk W. Directionally selective calcium signals in dendrites of starburst amacrine cells. Nature. 2002; 418:845–852. [PubMed: 12192402]

Famiglietti EV. Synaptic organization of starburst amacrine cells in rabbit retina: Analysis of serial thin sections by electron microscopy and graphic reconstruction. The Journal of Comparative Neurology. 1991; 309:40–70. [PubMed: 1894768]

Feldman ML, Peters A. The forms of non-pyramidal neurons in the visual cortex of the rat. The Journal of Comparative Neurology. 1978; 179:761–793. [PubMed: 346619]

Fisher SK. A somato-somatic synapse between amacrine and bipolar cells in the cat retina. Brain Research. 1972; 43:587–590. [PubMed: 5053291]

Fletcher EL, Hack I, Brandstätter JH, Wässle H. Synaptic localization of NMDA receptor subunits in the rat retina. The Journal of Comparative Neurology. 2000; 420:98–112. [PubMed: 10745222]

Frederick JM, Rayborn ME, Laties AM, Lam DM, Hollyfield JG. Dopaminergic neurons in the human retina. The Journal of Comparative Neurology. 1982; 210:65–79. [PubMed: 6127354]

Fujieda H, Sasaki H. Expression of brain-derived neurotrophic factor in cholinergic and dopaminergic amacrine cells in the rat retina and the effects of constant light rearing. Experimental Eye Research. 2008; 86:335–343. [PubMed: 18093585]

Gábriel R, Zhu B, Straznicky C. Tyrosine hydroxylase-like immunoreactive elements in the distal retina of Bufo marinus: A light and electron microscopic study. Brain Research. 1991; 539:225–232.

Gábriel R, Zhu B, Straznicky C. Synaptic contacts of tyrosine hydroxylase-immunoreactive elements in the inner plexiform layer of the retina of Bufo marinus. Cell and Tissue Research. 1992; 267:525–534. [PubMed: 1349266]

Gábriel R, de Souza S, Ziff EB, Witkovsky P. Association of the AMPA receptor-related postsynaptic density proteins GRIP and ABP with subsets of glutamate-sensitive neurons in the rat retina. The Journal of Comparative Neurology. 2002; 449:129–140. [PubMed: 12115684]

Geng Y, Schery LA, Sharma R, Dubra A, Ahmad K, Libby RT, Williams DR. Optical properties of the mouse eye. Biomedical Optics Express. 2011; 2:717–738. [PubMed: 21483598]

Ghosh KK, Haverkamp S, Wässle H. Glutamate receptors in the rod pathway of the mammalian retina. Journal of Neuroscience. 2001; 21:8636–8647. [PubMed: 11606651]

Graveland GA, Williams RS, DiFiglia M. A Golgi study of the human neostriatum: Neurons and afferent fibers. The Journal of Comparative Neurology. 1985; 234:317–333. [PubMed: 3988987]

Gray NW, Weimer RM, Bureau I, Svoboda K. Rapid redistribution of synaptic PSD-95 in the neocortex in vivo. PLoS Biology. 2006; 4(11):e370. [PubMed: 17090216]

Greferath U, Grünert U, Fritschy JM, Stephenson A, Möhler H, Wässle H. GABAA receptor subunits have differential distributions in the rat retina: In situ hybridization and immunohistochemistry. The Journal of Comparative Neurology. 1995; 353:553–571. [PubMed: 7759615]

Gründer T, Kohler K, Guenther E. Distribution and developmental regulation of AMPA receptor subunit proteins in rat retina. Investigative Ophthalmology & Visual Science. 2000; 41:3600–3606. [PubMed: 11006258]

Grünert U, Haverkamp S, Fletcher EL, Wässle H. Synaptic distribution of ionotropic glutamate receptors in the inner plexiform layer of the primate retina. The Journal of Comparative Neurology. 2002; 447:138–151. [PubMed: 11977117]

Grünert U, Jusuf PR, Lee SC, Nguyen DT. Bipolar input to melanopsin containing ganglion cells in primate retina. Visual Neurocience. 2011; 28:39–50.

Guimarães PZ, Hokoç JN. Tyrosine hydroxylase expression in the Cebus monkey retina. Visual Neurocience. 1997; 14:705–715.

Gustincich S, Feigenspan A, Wu DK, Koopman LJ, Raviola E. Control of dopamine release in the retina: A transgenic approach to neural networks. Neuron. 1997; 18:723–736. [PubMed: 9182798]

Häeggendal J, Malmfors T. Identification and cellular localization of the catecholamines in the retina and the choroid of the rabbit. Acta Physiologica. 1965; 64:58–66.

Hage TA, Sun Y, Khaliq ZM. Electrical and Ca^{2+} signaling in dendritic spines of substantia nigra dopaminergic neurons. Elife. 2016; 5:e13905. [PubMed: 27163179]

Hare WA, Owen WG. Similar effects of carbachol and dopamine on neurons in the distal retina of the tiger salamander. Visual Neurocience. 1995; 12:443–455.

Harris KM, Stevens JK. Dendritic spines of CA 1 pyramidal cells in the rat hippocampus: Serial electron microscopy with reference to their biophysical characteristics. Journal of Neuroscience. 1989; 9:2982–2997. [PubMed: 2769375]

Hartveit E. Functional organization of cone bipolar cells in the rat retina. Journal of Neurophysiology. 1997; 77:1716–1730. [PubMed: 9114231]

Hartveit E, Brandstätter JH, Sassoè-Pognetto M, Laurie DJ, Seeburg PH, Wässle H. Localization and developmental expression of the NMDA receptor subunit NR2A in the mammalian retina. The Journal of Comparative Neurology. 1994; 348:570–582. [PubMed: 7836563]

Haverkamp S, Grünert U, Wässle H. The cone pedicle, a complex synapse in the retina. Neuron. 2000; 27:85–95. [PubMed: 10939333]

Hokoç JN, Mariani AP. Tyrosine hydroxylase immunoreactivity in the rhesus monkey retina reveals synapses from bipolar cells to dopaminergic amacrine cells. Journal of Neuroscience. 1987; 7:2785–93. [PubMed: 2887643]

Hokoç JN, Mariani AP. Synapses from bipolar cells onto dopaminergic amacrine cells in cat and rabbit retinas. Brain Research. 1988; 461:17–26. [PubMed: 2906268]

Holmgren I. Synaptic organization of the dopaminergic neurons in the retina of the cynomolgus monkey. Investigational Ophthalmology & Visual Science. 1982; 22:8–24.

Hoshi H, Liu WL, Massey SC, Mills SL. ON inputs to the OFF layer: Bipolar cells that break the stratification rules of the retina. Journal of Neuroscience. 2009; 29:8875–8883. [PubMed: 19605625]

Inanobe A, Yoshimoto Y, Horio Y, Morishige KI, Hibino H, Matsumoto S, Kurachi Y. Characterization of G-protein-gated K + channels composed of Kir3.2 subunits in dopaminergic neurons of the substantia nigra. Journal of Neuroscience. 1999; 19:1006–1017. [PubMed: 9920664]

Jaffe EH, Marty A, Schulte A, Chow RH. Extrasynaptic vesicular transmitter release from the somata of substantia nigra neurons in rat midbrain slices. Journal of Neuroscience. 1998; 18:3548–3553. [PubMed: 9570786]

Jakobs TC, Ben Y, Masland RH. CD15 immunoreactive amacrine cells in the mouse retina. The Journal of Comparative Neurology. 2003; 465:361–371. [PubMed: 12966561]

Jang M, Um KB, Jang J, Kim HJ, Cho H, Chung S, Park MK. Coexistence of glutamatergic spine synapses and shaft synapses in substantia nigra dopamine neurons. Scientific Reports. 2015; 5:14773. [PubMed: 26435058]

Jones EG, Powell TP. Morphological variations in the dendritic spines of the neocortex. Journal of Cell Science. 1969; 5:509–529. [PubMed: 5362339]

Jones BW, Marc RE, Watt CB. Dopaminergic amacrine and interplexiform cells exhibit glutamatergic signatures. Invetigational Ophthalmology & Visual Science. 2004; 45 ARVO E-abstract #5435.

Keeley PW, Reese BE. Morphology of dopaminergic amacrine cells in the mouse retina: Independence from homotypic interactions. The Journal of Comparative Neurology. 2010; 518:1220–1231. [PubMed: 20148440]

Kirsch M, Wagner HJ. Release pattern of endogenous dopamine in teleost retinae during light adaptation and pharmacological stimulation. Vision Research. 1989; 29:147–154. [PubMed: 2800344]

Kolb H, Cline C, Wang HH, Brecha N. Distribution and morphology of dopaminergic amacrine cells in the retina of the turtle (*Pseudemys scripta elegans*). Journal of Neurocytology. 1987; 16:577–588. [PubMed: 2891796]

Kolb H, Cuenca N, Wang HH, Dekorver L. The synaptic organization of the dopaminergic amacrine cell in the cat retina. Journal of Neurocytology. 1990; 19:343–366. [PubMed: 2391538]

Kolb H, Cuenca N, Dekorver L. Postembedding immunocytochemistry for GABA and glycine reveals the synaptic relationships of the dopaminergic amacrine cell of the cat retina. The Journal of Comparative Neurology. 1991; 310:267–284. [PubMed: 1720142]

Kolb H, Netzer E, Ammermüller J. Neural circuitry and light responses of the dopamine amacrine cell of the turtle retina. Molecular Vision. 1997; 3:6. [PubMed: 9238095]

Kolbinger W, Weiler R. Modulation of endogenous dopamine release in the turtle retina: Effects of light, calcium, and neurotransmitters. Visual Neurocience. 1993; 10:1035–1041.

Kornau HC, Schenker LT, Kennedy MB, Seeburg PH. Domain interaction between NMDA receptor subunits and the postsynaptic density protein PSD-95. Science. 1995; 269:1737–1740. [PubMed: 7569905]

Koulen P, Fletcher EL, Craven SE, Bredt DS, Wässle H. Immunocytochemical localization of the postsynaptic density protein PSD-95 in the mammalian retina. Journal of Neuroscience. 1998; 18:10136–10149. [PubMed: 9822767]

Kouvidi E, Papadopoulou-Daifoti Z, Thermos K. Somatostatin modulates dopamine release in rat retina. Neuroscience Letters. 2006; 391:82–86. [PubMed: 16183196]

Kramer SG. Dopamine: A retinal neurotransmitter. I. Retinal uptake, storage, and light-stimulated release of H3-dopamine in vivo. Investigative Ophthalmology. 1971; 10:438–452. [PubMed: 4325307]

Lasansky A. Lateral contacts and interactions of horizontal cell dendrites in the retina of the larval tiger salamander. Journal of Physiology. 1980; 301:59–68. [PubMed: 7411448]

Lin B, Masland RH. Populations of wide-field amacrine cells in the mouse retina. The Journal of Comparative Neurology. 2006; 499:797–809. [PubMed: 17048228]

Lin B, Martin PR, Grünert U. Expression and distribution of ionotropic glutamate receptor subunits on parasol ganglion cells in the primate retina. Visual Neurocience. 2002; 19:453–465.

Linberg KA, Fisher SK. An ultrastructural study of interplexiform cell synapses in the human retina. The Journal of Comparative Neurology. 1986; 243:561–576. [PubMed: 3950087]

Liu Y, Lee JW, Ackerman SL. Mutations in the microtubule-associated protein 1A (Map1a) gene cause Purkinje cell degeneration. Journal of Neuroscience. 2015; 35:4587–4598. [PubMed: 25788676]

Marc, RE. Functional neuroanatomy of the retina. In: Albert, DM.Miller, JW.Azar, DR., Blodi, BA., editors. Albert and Jakobiec's Principles and Practice of Ophthalmology. 3. New York, NY: Elsevier; 2008. p. 1565-1592.

Marc RE, Liu WLS. Horizontal cell synapses onto glycine-accumulating interplexiform cells. Nature. 1984; 312:266–269. [PubMed: 6504139]

Mariani AP. Amacrine cells of the rhesus monkey retina. The Journal of Comparative Neurology. 1990; 301:382–400. [PubMed: 2262597]

Mariani AP, Hokoç JN. Two types of tyrosine hydroxylase-immunoreactive amacrine cell in the rhesus monkey retina. The Journal of Comparative Neurology. 1988; 276:81–91. [PubMed: 2903868]

Mariani AP, Kolb H, Nelson R. Dopamine-containing amacrine cells of rhesus monkey retina parallel rods in spatial distribution. Brain Research. 1984; 322:1–7. [PubMed: 6518360]

Matsuzaki M, Ellis-Davies GC, Nemoto T, Miyashita Y, Iino M, Kasai H. Dendritic spine geometry is critical for AMPA receptor expression in hippocampal CA1 pyramidal neurons. Nature Neuroscience. 2001; 4:1086–1092. [PubMed: 11687814]

Megaw PL, Boelen MG, Morgan IG, Boelen MK. Diurnal patterns of dopamine release in chicken retina. Neurochemistry International. 2006; 48:17–23. [PubMed: 16188347]

Mitrofanis J, Provis JM. A distinctive soma size gradient among catecholaminergic neurones of human retinae. Brain Research. 1990; 527:69–75. [PubMed: 1980840]

Mitrofanis J, Vigny A, Stone J. Distribution of catecholaminergic cells in the retina of the rat, guinea pig, cat, and rabbit: Independence from ganglion cell distribution. The Journal of Comparative Neurology. 1988; 267:1–14. [PubMed: 2893816]

Morigiwa K, Vardi N. Differential expression of ionotropic glutamate receptor subunits in the outer retina. The Journal of Comparative Neurology. 1999; 405:173–184. [PubMed: 10023808]

Nakamura Y, McGuire BA, Sterling P. Interplexiform cell in cat retina: identification by uptake of gamma-[3H]aminobutyric acid and serial reconstruction. Proceedings of the National Academy of Sciences of the United States of America. 1980; 77:658–661. [PubMed: 6928650]

Negishi K, Kato S, Teranishi T, Kiyama H, Katayama Y, Tohyama M. So-called interplexiform cells immunoreactive to tyrosine hydroxylase or somatostatin in rat retina. Brain Research. 1985; 346:136–140. [PubMed: 2864980]

Newkirk GS, Moon M, Wong RO, Detwiler PB. Inhibitory inputs tune the light response properties of dopaminergic amacrine cells in mouse retina. Journal of Neurophysiology. 2013; 110:536–552. [PubMed: 23636722]

Nguyen-Legros J, Berger B, Vigny A, Alvarez C. Tyrosine hydroxylase-like immunoreactive interplexiform cells in the rat retina. Neuroscience Letters. 1981; 27:255–259. [PubMed: 6120490]

Nguyen-Legros J, Moussafi F, Simon A. Sclerally directed processes of dopaminergic interplexiform cells reach the outer nuclear layer in rat and monkey retina. Visual Neurocience. 1990; 4:547–553.

Nguyen-Legros J, Versaux-Botteri C, Savy C. Dopaminergic and GABAergic retinal cell populations in mammals. Microscopy Research and Technique. 1997; 36:26–42. [PubMed: 9031259]

O'Brien RJ, Kamboj S, Ehlers MD, Rosen KR, Fischbach GD, Huganir RL. Activity-dependent modulation of synaptic AMPA receptor accumulation. Neuron. 1998; 21:1067–1078. [PubMed: 9856462]

O'Connor P, Dorison SJ, Watling KJ, Dowling JE. Factors affecting release of 3H-dopamine from perfused carp retina. Journal of Neuroscience. 1986; 6:1857–1865. [PubMed: 2874198]

Østergaard J, Hannibal J, Fahrenkrug J. Synaptic contact between melanopsin-containing retinal ganglion cells and rod bipolar cells. Invetigational Ophthalmology & Visual Science. 2007; 48:3812–3820.

Overton P, Clark D. Iontophoretically administered drugs acting at the N-methyl-D-aspartate receptor modulate burst firing in A9 dopamine neurons in the rat. Synapse. 1992; 10:131–140. [PubMed: 1533955]

Oyster CW, Takahashi ES, Cilluffo M, Brecha NC. Morphology and distribution of tyrosine hydroxylase-like immunoreactive neurons in the cat retina. Proceedings of the National Academy of Science of the United States of America. 1985; 82:6335–6339.

Pallotto M, Watkins PV, Fubara B, Singer JH, Briggman KL. Extracellular space preservation aids the connectomic analysis of neural circuits. Elife. 2015; 4:e08206. [PubMed: 26650352]

Partida GJ, Lee SC, Haft-Candell L, Nichols GS, Ishida AT. DARPP-32-like immunoreactivity in AII amacrine cells of rat retina. The Journal of Comparative Neurology. 2004; 480:251–263. [PubMed: 15515184]

Peichl L, González-Soriano J. Morphological types of horizontal cell in rodent retinae: A comparison of rat, mouse, gerbil, and guinea pig. Visual Neurocience. 1994; 11:501–517.

Peng YW, Blackstone CD, Huganir RL, Yau KW. Distribution of glutamate receptor subtypes in the vertebrate retina. Neuroscience. 1995; 66:483–497. [PubMed: 7477889]

Peters A, Kaiserman-Abramof IR. The small pyramidal neuron of the rat cerebral cortex. The perikaryon, dendrites and spines. American Journal of Anatomy. 1970; 127:321–355. [PubMed: 4985058]

Petralia RS, Esteban JA, Wang YX, Partridge JG, Zhao HM, Wenthold RJ, Malinow R. Selective acquisition of AMPA receptors over postnatal development suggests a molecular basis for silent synapses. Nature Neuroscience. 1999; 2:31–36. [PubMed: 10195177]

Piccolino M, Witkovsky P, Trimarchi C. Dopaminergic mechanisms underlying the reduction of electrical coupling between horizontal cells of the turtle retina induced by d-amphetamine, bicuculline, and veratridine. Journal of Neuroscience. 1987; 8:2273–2284.

Pollard J, Eldred WD. Synaptic analysis of amacrine cells in the turtle retina which contain tyrosine hydroxylase-like immunoreactivity. Journal of Neurocytology. 1990; 19:53–66. [PubMed: 1972186]

Pourcho RG. Dopaminergic amacrine cells in the cat retina. Brain Research. 1982; 252:101–109. [PubMed: 7172014]

Preibisch S, Saalfeld S, Tomancak P. Globally optimal stitching of tiled 3D microscopic image acquisitions. Bioinformatics. 2009; 25:1463–1465. [PubMed: 19346324]

Prensa L, Cossette M, Parent A. Dopaminergic innervation of human basal ganglia. Journal of Chemical Neuroanatomy. 2000; 20:207–213. [PubMed: 11207419]

Puopolo M, Hochstetler SE, Gustincich S, Wightman RM, Raviola E. Extrasynaptic release of dopamine in a retinal neuron: Activity dependence and transmitter modulation. Neuron. 2001; 30:211–225. [PubMed: 11343656]

Qin P, Pourcho RG. AMPA-selective glutamate receptor subunits GluR2 and GluR4 in the cat retina: An immunocytochemical study. Visual Neurocience. 1999; 16:1105–1114.

Röhrenbeck J, Wässle H, Heizmann CW. Immunocytochemical labelling of horizontal cells in mammalian retina using antibodies against calcium-binding proteins. Neuroscience Letters. 1987; 77:255–260. [PubMed: 3302765]

Sakai H, Naka K. Novel pathway connecting the outer and inner vertebrate retina. Nature. 1985; 315:570–571. [PubMed: 2409445]

Sarthy PV, Lam DM. The uptake and release of [3H]dopamine in the goldfish retina. Journal of Neurochemistry. 1979; 32:1269–1277. [PubMed: 430085]

Savy C, Moussafi F, Durand J, Yelnik J, Simon A, Nguyen-Legros J. Distribution and spatial geometry of dopamine interplexiform cells in the retina. II. External arborizations in the adult rat and monkey. The Journal of Comparative Neurology. 1995; 355:392–404. [PubMed: 7636021]

Schmitz F, Königstorfer A, Südhof TC. RIBEYE, a component of synaptic ribbons: A protein's journey through evolution provides insight into synaptic ribbon function. Neuron. 2000; 28:857–872. [PubMed: 11163272]

Schütte M, Witkovsky P. Dopaminergic interplexiform cells and centrifugal fibres in the Xenopus retina. Journal of Neurocytology. 1991; 20:195–207. [PubMed: 1674751]

Sheng M, Kim E. The postsynaptic organization of synapses. Cold Spring Harbor Perspectives in Biology. 2011; 3:a005678. [PubMed: 22046028]

Sherry DM, Wang MM, Bates J, Frishman LJ. Expression of vesicular glutamate transporter 1 in the mouse retina reveals temporal ordering in development of rod vs. cone and ON vs. OFF circuits. The Journal of Comparative Neurology. 2003; 465:480–498. [PubMed: 12975811]

Siegel SJ, Janssen WG, Tullai JW, Rogers SW, Moran T, Heinemann SF, Morrison JH. Distribution of the excitatory amino acid receptor subunits GluR2(4) in monkey hippocampus and colocalization with subunits GluR5–7 and NMDAR1. Journal of Neuroscience. 1995; 15:2707–2719. [PubMed: 7722624]

Slaughter MM, Miller RF. 2-amino-4-phosphonobutyric acid: A new pharmacological tool for retina research. Science. 1981; 211:182–185. [PubMed: 6255566]

Stell WK, Lightfoot DO. Color-specific interconnections of cones and horizontal cells in the retina of the goldfish. The Journal of Comparative Neurology. 1975; 159:473–502. [PubMed: 1092733]

Stradleigh TW, Ogata G, Partida GJ, Oi H, Greenberg KP, Krempely KS, Ishida AT. Colocalization of hyperpolarization-activated, cyclic nucleotide-gated channel subunits in rat retinal ganglion cells. The Journal of Comparative Neurology. 2011; 519:2546–2573. [PubMed: 21456027]

Stradleigh TW, Greenberg KP, Partida GJ, Pham A, Ishida AT. Moniliform deformation of retinal ganglion cells by formaldehyde-based fixatives. The Journal of Comparative Neurology. 2015; 523:545–564. [PubMed: 25283775]

Susaki EA, Tainaka K, Perrin D, Yukinaga H, Kuno A, Ueda HR. Advanced CUBIC protocols for whole-brain and whole-body clearing and imaging. Nature Protocols. 2015; 10:1709–1727. [PubMed: 26448360]

Tamura N, Yokotani K, Okuma Y, Okada M, Ueno H, Osumi Y. Properties of the voltage-gated calcium channels mediating dopamine and acetylcholine release from the isolated rat retina. Brain Research. 1995; 676:363–370. [PubMed: 7614007]

Tauchi M, Madigan NK, Masland RH. Shapes and distributions of the catecholamine-accumulating neurons in the rabbit retina. The Journal of Comparative Neurology. 1990; 293:178–189. [PubMed: 19189710]

Taylor WR. Response properties of long-range axon-bearing amacrine cells in the dark-adapted rabbit retina. Visual Neurocience. 1996; 13:599–604.

Teakle EM, Wildsoet CF, Vaney DI. The spatial organization of tyrosine hydroxylase-immunoreactive amacrine cells in the chicken retina and the consequences of myopia. Vision Research. 1993; 33:2383–2396. [PubMed: 7902629]

tom Dieck S, Altrock WD, Kessels MM, Qualmann B, Regus H, Brauner D, Brandstätter JH. Molecular dissection of the photoreceptor ribbon synapse: Physical interaction of Bassoon and RIBEYE is essential for the assembly of the ribbon complex. Journal of Cell Biology. 2005; 168:825–836. [PubMed: 15728193]

van Haesendonck E, Marc RE, Missotten L. New aspects of dopaminergic interplexiform cell organization in the goldfish retina. The Journal of Comparative Neurology. 1993; 333:503–518. [PubMed: 8103778]

Versaux-Botteri C, Nguyen-Legros J, Vigny A, Raoux N. Morphology, density and distribution of tyrosine hydroxylase-like immunoreactive cells in the retina of mice. Brain Research. 1984; 301:192–197. [PubMed: 6145503]

Vinade L, Chang M, Schlief ML, Petersen JD, Reese TS, Tao-Cheng JH, Dosemeci A. Affinity purification of PSD-95-containing postsynaptic complexes. Journal of Neurochemistry. 2003; 87:1255–1261. [PubMed: 14622105]

Voigt T, Wässle H. Dopaminergic innervation of A II amacrine cells in mammalian retina. Journal of Neuroscience. 1987; 7:4115–4128. [PubMed: 2891802]

Vuong HE, Hardi CN, Barnes S, Brecha NC. Parallel inhibition of dopamine amacrine cells and intrinsically photosensitive retinal ganglion cells in a non-image-forming visual circuit of the mouse retina. Journal of Neuroscience. 2015; 35:15955–15970. [PubMed: 26631476]

Wahlin KJ, Moreira EF, Huang H, Yu N, Adler R. Molecular dynamics of photoreceptor synapse formation in the developing chick retina. The Journal of Comparative Neurology. 2008; 506:822–837. [PubMed: 18076030]

Wässle H, Grünert U, Röhrenbeck J. Immunocytochemical staining of AII-amacrine cells in the rat retina with antibodies against parvalbumin. The Journal of Comparative Neurology. 1993; 332:407–420. [PubMed: 8349840]

Wenthold RJ, Yokotani N, Doi K, Wada K. Immunochemical characterization of the non-NMDA glutamate receptor using subunit-specific antibodies. Evidence for a hetero-oligomeric structure in rat brain. The Journal of Biological Chemistry. 1992; 267:501–507. [PubMed: 1309749]

Westrum LE. Observations on initial segments of axons in the prepyriform cortex of the rat. The Journal of Comparative Neurology. 1970; 139:337–356. [PubMed: 4914800]

Witkovsky P, Dearry A. Functional roles of dopamine in the vertebrate retina. Progress in Retinal Research. 1991; 11:247–292.

Witkovsky P, Zhang J, Blam O. Dopaminergic neurons in the retina of Xenopus laevis: Amacrine vs. interplexiform subtypes and relation to bipolar cells. Cell and Tissue Research. 1994; 278:45–56. [PubMed: 7954703]

Witkovsky P, Veisenberger E, Haycock JW, Akopian A, Garcia-Espana A, Meller E. Activity-dependent phosphorylation of tyrosine hydroxylase in dopaminergic neurons of the rat retina. Journal of Neuroscience. 2004; 24:4242–4249. [PubMed: 15115820]

Witkovsky P, Arango-Gonzalez B, Haycock JW, Kohler K. Rat retinal dopaminergic neurons: Differential maturation of somatodendritic and axonal compartments. The Journal of Comparative Neurology. 2005; 481:352–362. [PubMed: 15593337]

Witkovsky P, Shen CP, McRory J. Differential distribution of voltage-gated calcium channels in dopaminergic neurons of the rat retina. The Journal of Comparative Neurology. 2006; 497:384–396. [PubMed: 16736476]

Witkovsky P, Gábriel R, Krizaj D. Anatomical and neurochemical characterization of dopaminergic interplexiform processes in mouse and rat retinas. The Journal of Comparative Neurology. 2008; 510:158–174. [PubMed: 18615559]

Xu HP, Zhao JW, Yang XL. Cholinergic and dopaminergic amacrine cells differentially express calcium channel subunits in the rat retina. Neuroscience. 2003; 118:763–768. [PubMed: 12710983]

Yazulla S, Studholme KM. Glycinergic interplexiform cells make synaptic contact with amacrine cell bodies in goldfish retina. The Journal of Comparative Neurology. 1991; 310:1–10. [PubMed: 1658087]

Yazulla S, Zucker CL. Synaptic organization of dopaminergic interplexiform cells in the goldfish retina. Visual Neurocience. 1988; 1:13–29.

Zhang DQ, Stone JF, Zhou T, Ohta H, McMahon DG. Characterization of genetically labeled catecholamine neurons in the mouse retina. Neuroreport. 2004; 15:1761–1765. [PubMed: 15257143]

Zhang DQ, Zhou TR, McMahon DG. Functional heterogeneity of retinal dopaminergic neurons underlying their multiple roles in vision. Journal of Neuroscience. 2007; 27:692–699. [PubMed: 17234601]

Zhang DQ, Wong KY, Sollars PJ, Berson DM, Pickard GE, McMahon DG. Intraretinal signaling by ganglion cell photoreceptors to dopaminergic amacrine neurons. Proceeding of the National Academy of Science of the United State of America. 2008; 105:14181–14186.

Zhang J, Diamond JS. Distinct perisynaptic and synaptic localization of NMDA and AMPA receptors on ganglion cells in rat retina. The Journal of Comparative Neurology. 2006; 498:810–820. [PubMed: 16927255]

Zhu B, Straznicky C. Dendritic morphology and retinal distribution of tyrosine hydroxylase-like immunoreactive amacrine cells in Bufo marinus. Anatomy and Embryology. 1990; 181:365–371. [PubMed: 1971740]

Zucker CL, Dowling JE. Centrifugal fibres synapse on dopaminergic interplexiform cells in the teleost retina. Nature. 1987; 330:166–168. [PubMed: 2890106]

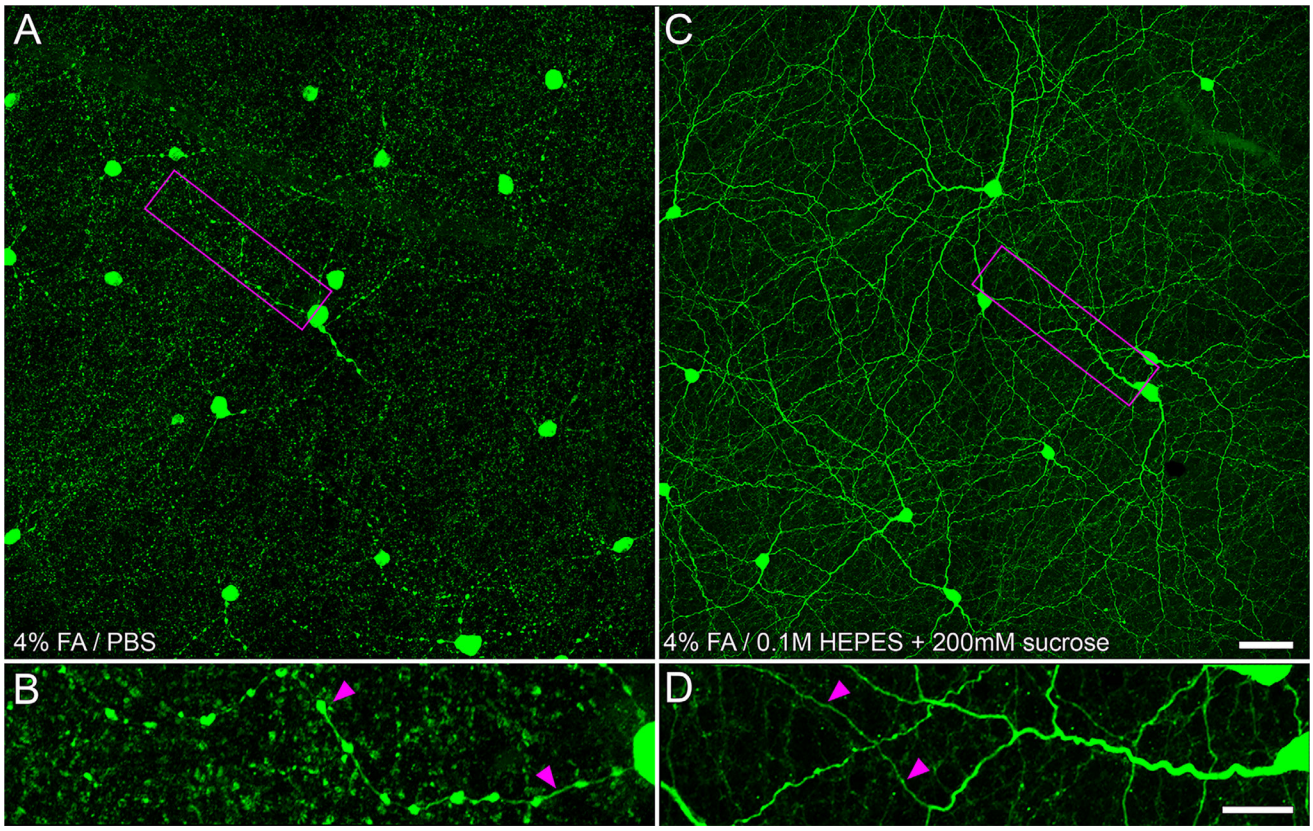

FIGURE 1.

Tyrosine hydroxylase (TH) cell segmentation versus preservation. TH-immunopositive somata and neurites (green) in flat-mounted retinae fixed by immersion in 4% formaldehyde (A,B) or sucrose-supplemented 4% formaldehyde (C,D). Z-projections (thickness = 30 μm) of optical sections through the inner nuclear, inner plexiform, and ganglion cell layers (abbreviated in figure legends hereafter as INL, IPL, and GCL, respectively). (A) Largest round TH-immunopositive profiles are somata (n = 19 in this field). Heavily beaded neurites extend away from some of these somata (e. g., along course framed in box). Other TH-immunopositive elements are small, segmented spots. (B) Field outlined by box in A, at higher magnification, showing varicose neurite (arrowheads) extending away from edge of soma, thin neuritic segments connecting the varicosities, and background of small TH-immunopositive spots. (C) TH-immunopositive neurites extending away from TH cell somata (n = 12 in this field) and overlapping neurites of other TH cells. Neurites emerging from somata are generally thick and smoothly contoured, and taper before the first branch point (e. g., along course framed in box). Other neurites are nontapering and varicose. (D) Field outlined by box in C at higher magnification, showing tapering neurite extending away from edge of soma, and thin varicose neurite (arrowheads) emerging at a third-order branch point. Scale bar = 50 μm in C (applies to A,C); 20 μm in D (applies to B,D)

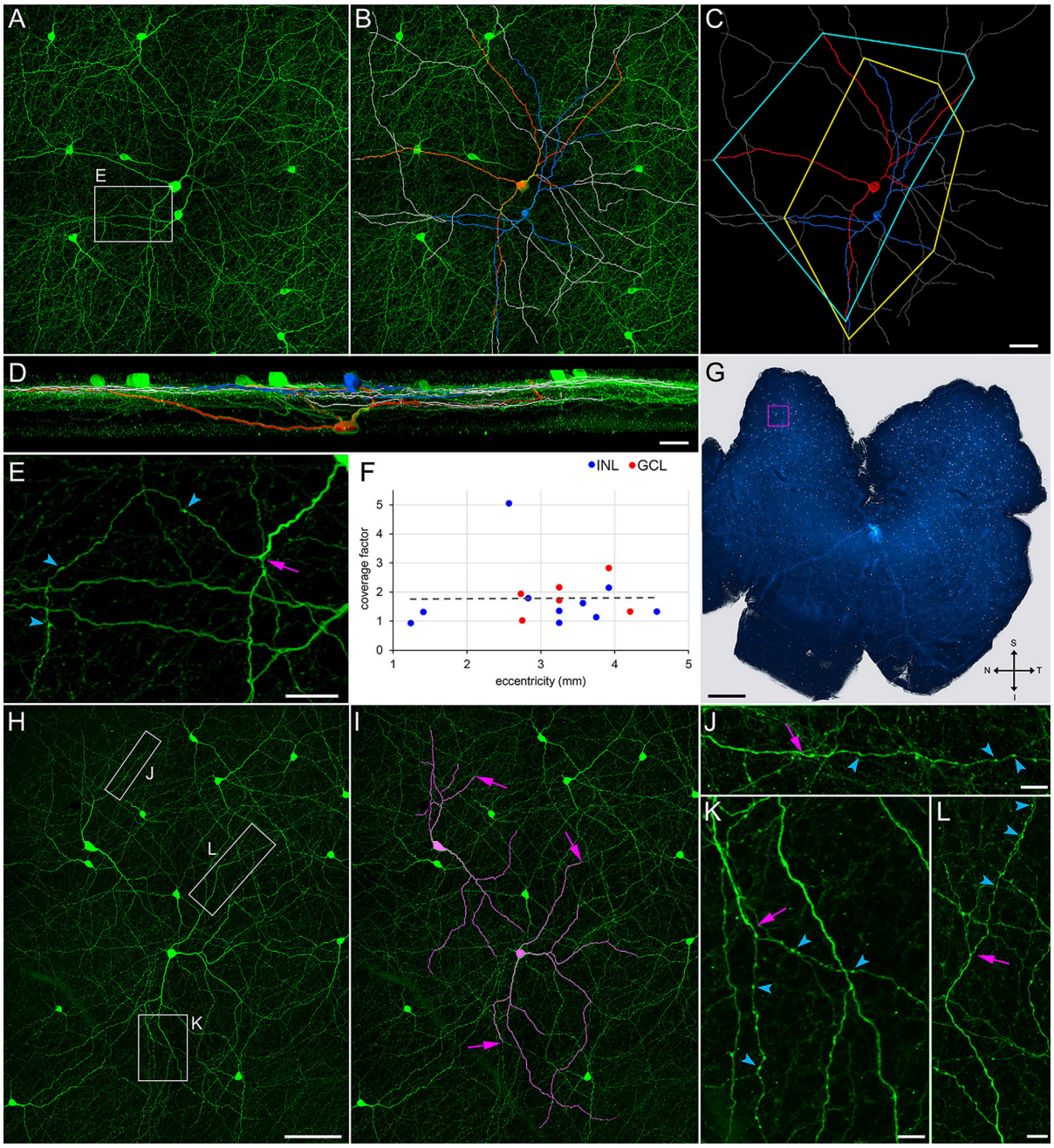

FIGURE 2.

Coverage factors. Flat-mounted retina (G) immunostained for TH (green). (A–D) Field marked by magenta square in G. (A) Z-projection (thickness = 71.5 μm) of optical sections through the INL, IPL, GCL, and nerve fiber layer. (B) Superimposition, on A, of tracings of (in blue) a TH cell soma in the INL and its tapering neurites, (in red) a TH cell soma in the GCL and its tapering neurites, and (in gray) the varicose neurites of these cells. (C) Tracings with no background, together with polygons that connect the tips of the tapering neurites. (D) 90 ° rotation of B. (E) Higher magnification display of field outlined by rectangle (labeled E) in A, showing termination (arrow) of a tapering neurite and emergence of a

varicose neurite as a side branch. (F) Coverage factors measured for cells with soma in the INL (blue dots) or GCL (red dots), at eccentricities 1 to 5 mm from optic nerve head in a total of six different retinae. Optic nerve head in G is light area near center of retina. (H) TH cells at an eccentricity of 3.25 mm in the inferior–temporal quadrant of a different retina than G. (I) Tapering neurites of two of these cells are highlighted in magenta. (J–L) Varicose neurites extending beyond the tip of these tapering neurites, within the areas outlined by the correspondingly lettered boxes in H. Arrows in I (and arrows at corresponding positions in J–L) point at end of tapering portions, and beginning of varicose portions, of neurites. Arrowheads point at a few varicosities in each neurite (E, J–L). Scale bar = 50 μm in C (applies to A–C); 30 μm, 25 μm, and 1 mm in D, E, and G, respectively; 100 μm in H (applies to H,I); 10 μm in J–L

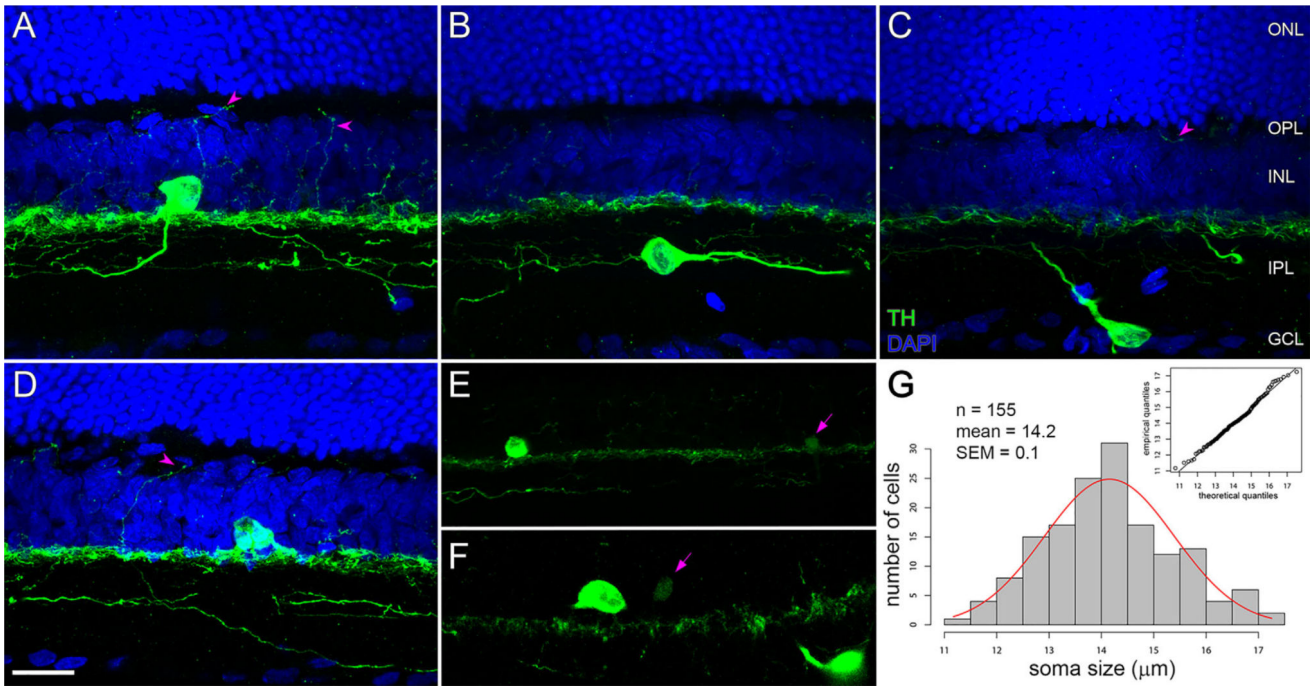

FIGURE 3.

TH cell variety. Vertical sections of retinae immunostained for TH (green) and counterstained for DAPI (blue). (A–F) Z-projections (17.48, 16.10, 9.45, 19.32, 8.55, and 5.85 μm in thickness, respectively). Levels of the INL, IPL, GCL, outer plexiform layer (OPL) and outer nuclear layer (ONL) are labeled in C and apply to A–D. (A) Interplexiform TH cell in the superior retina, with TH-immunopositive neurite ascending from the soma toward the OPL (left arrowhead) and immunopositive neurites arborizing in distal, intermediate, and proximal sublayers of the IPL. Another immunopositive neurite (right arrowhead) extends between the IPL and OPL. (B) TH cell with soma within the IPL. Note thin, varicose neurite extending from the soma toward the left side of B, and thick tapering neurite extending from the soma toward the right side of B. (C) TH cell with soma in GCL, with thick tapering neurite extending toward the distal sublayer of the IPL. Arrowhead points to TH-immunopositive segment in the OPL. (D) TH cell in the inferior retina with soma in the INL. Arrowhead points to TH-immunopositive process extending between the IPL and OPL. (E,F) Brightly and dimly fluorescing TH cell somata. Each panel shows one of each to contrast these at identical imaging settings. Arrows point at dim TH cell somata. (G) Histogram of TH cell soma sizes. Means of maximum and minimum Feret's diameters of bright somata in the INL in flat-mounted retinae. Inset is Q-Q plot comparing the quantiles of the measured diameters (ordinate) with quantiles of a standard normal population (abscissa). Points are near unity line (continuous line), indicating that diameters are normally distributed. Scale bar = 20 μm in D (applies to A–F)

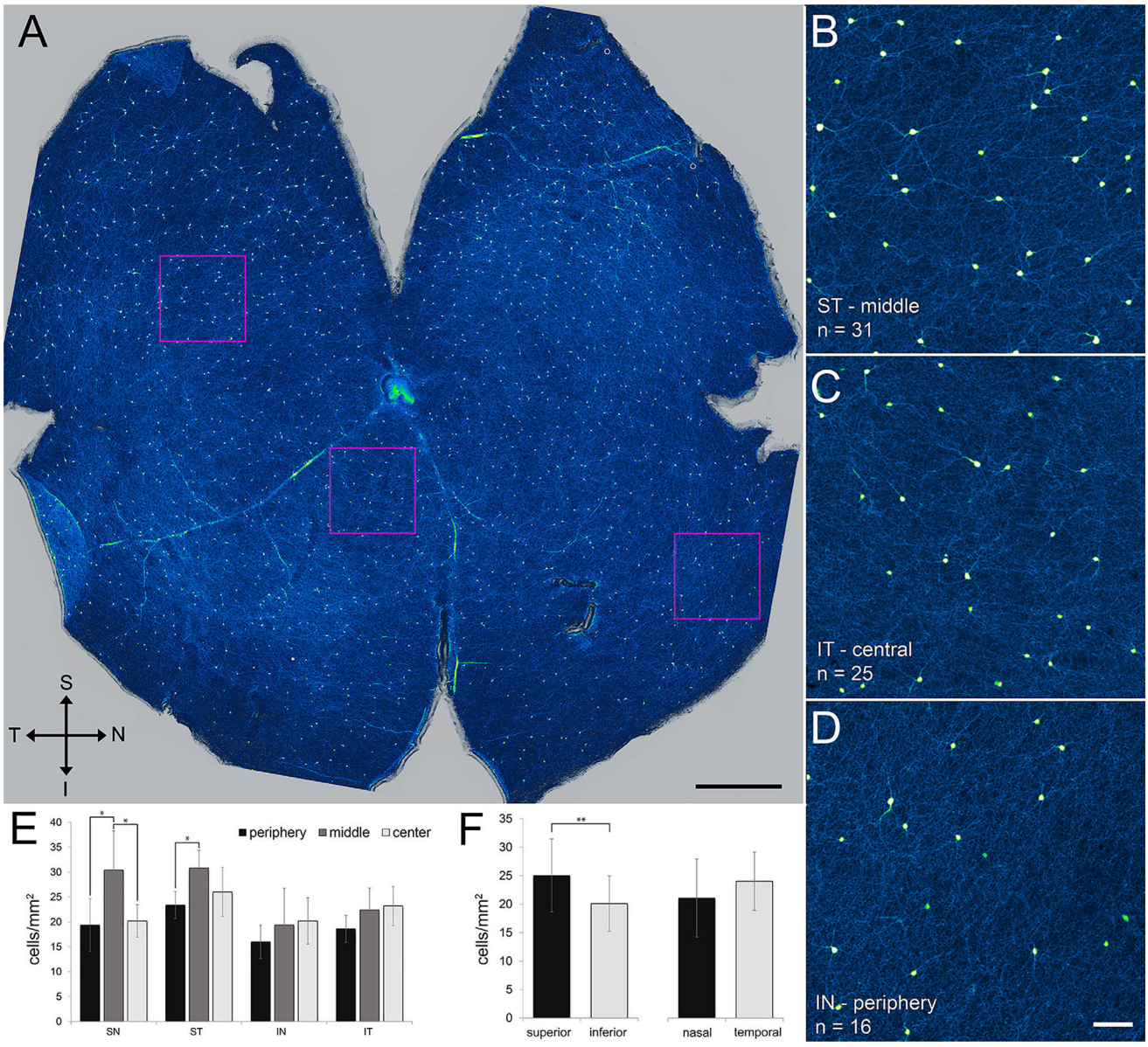

FIGURE 4.

TH cell distribution and density. (A) Flat-mounted retina immunostained for TH (green–yellow). Images collected at 4× and stitched with Fiji. Superior, inferior, temporal, and nasal directions as marked (S, I, T, N). Optic nerve head is light area near center of retina. (B–D) Higher magnification displays of fields outlined by squares in A. TH-immunopositive neurites can be seen extending away from several of the somata. Cell density is cell count (*n*) in each field divided by field size (1 mm^2). (E,F) Numbers of cells in 1-mm^2 fields from three eccentricities (central, middle, peripheral) in all quadrants (superior-temporal, superior-nasal, inferior-temporal, inferior-nasal) in all retinae prepared as in A ($n = 5$). Cell counts are significantly higher in midperipheral eccentricities of the superior retina than at central or peripheral eccentricities (E; SN: periphery vs. middle, $p = 0.028$; center vs. middle, $p = 0.041$; ST: periphery vs. middle, $p = 0.026$; one-way ANOVA followed by

Tukey's post hoc test). Cell counts are higher in superior hemiretina than in inferior hemiretina (F; $p = 0.002$; unpaired t test). Cell counts do not significantly differ with eccentricity in inferior retina (E) or between nasal and temporal hemiretinae (F). Scale bar = 1 mm in A; 100 μm in D (applies to B–D)

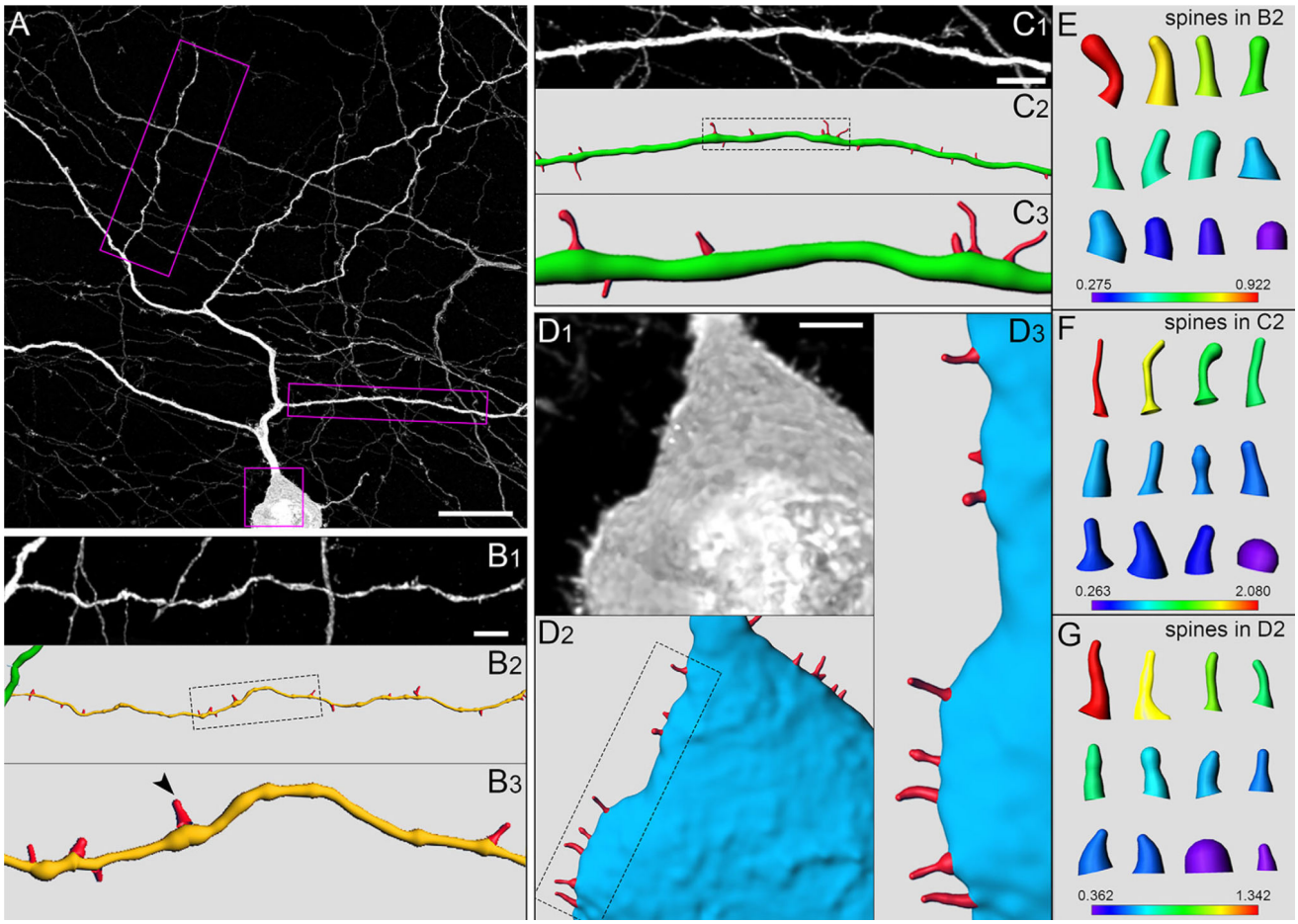

FIGURE 5.

Spines (Long–Evans rat). (A) Portion of TH cell soma (in GCL) and neuritic arbor in flat-mounted retina, oversampled during confocal imaging and deconvolved. Z-projection (thickness = 7.65 μm) of optical sections through the proximal IPL and GCL. (B–D) Higher magnification and reconstruction of varicose neurite (B1–B3), tapering neurite (C1–C3), and soma (D1–D3). (B1,C1,D1) Regions outlined by boxes in A. (B2,C2,D2) Digital reconstructions of soma and neurite in B1, C1, and D1. (B3,C3,D3) Regions outlined by dotted lines in B2, C2, and D2, respectively. Arrowhead in B3 points at spine extending out from varicosity. (E–G) Reconstructions of some spines in B2, C2, and D2, respectively, including spines on the distal and sclerad faces (above and below the plane of the panels). Axial length (in μm) of each spine in E, F, and G is indicated by matching color along heat bars. Scale bar = 20 μm in A; 5 μm in B1; 5 μm in C1; 3 μm in D1

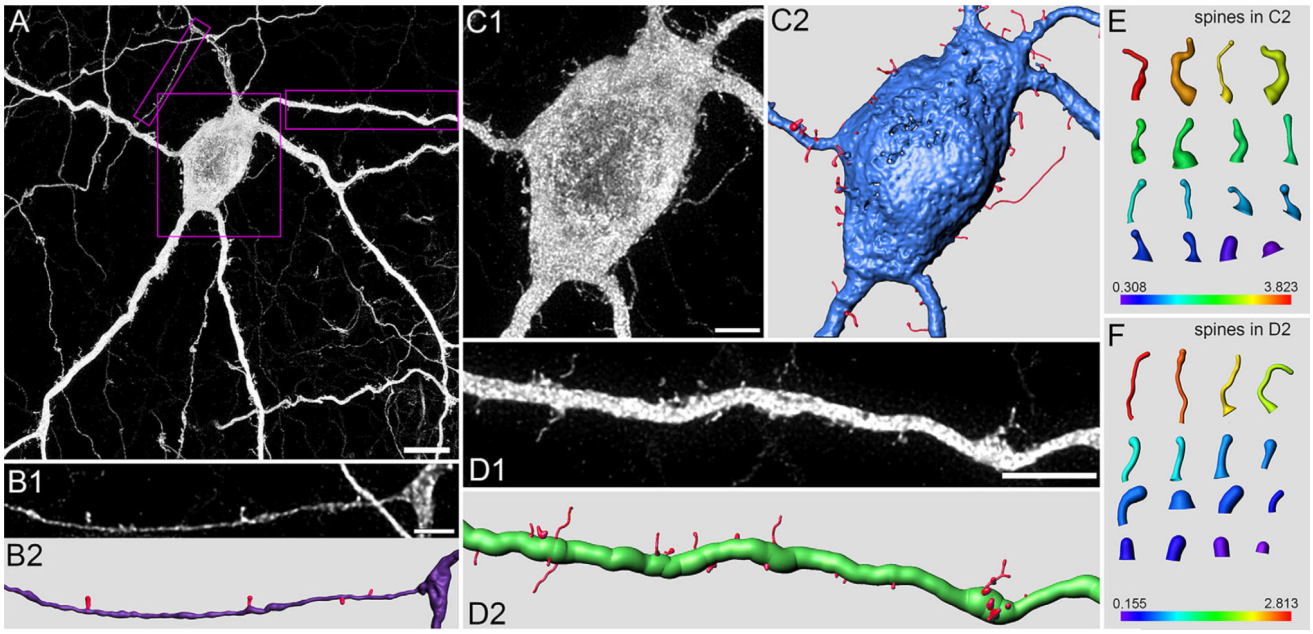

FIGURE 6.

Spines (Lewis rat). (A) Portion of TH cell soma (in the GCL) and neuritic arbor in flat-mounted retina, oversampled during confocal imaging and deconvolved. Z-projection (thickness = 12.78 μm) of optical sections through the proximal IPL and GCL. Higher magnification and reconstruction of varicose neurite (B1,B2), soma (C1,C2), and tapering neurite (D1,D2). (B1,C1,D1) Regions outlined by boxes in A. (B2,C2,D2) Digital reconstructions of soma and neurites in B1, C1, and D1. (E,F) Reconstructions of some spines in C2 and D2, respectively, including spines on the distal and sclerad faces (above and below the plane of the panels). Axial length (in μm) of each spine in E and F is indicated by matching color along heat bars. Scale bar = 10 μm in A; 2 μm in B1; 5 μm in C1; 10 μm in D1

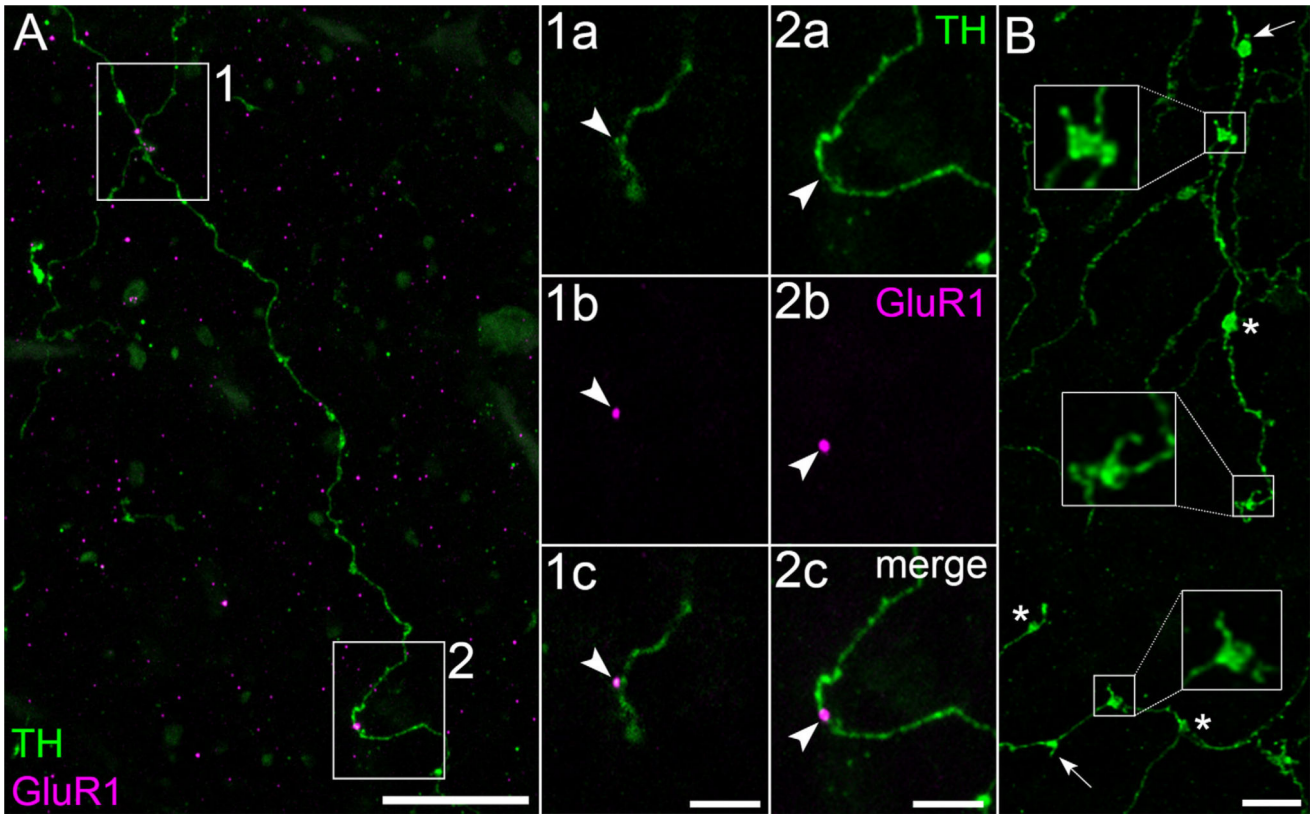

FIGURE 7.

GluR1 and spine-bearing varicosities in OPL. (A) Portions of TH cell varicose neurite (green) in the OPL of flat-mounted retina. Z-projection (thickness = 9.2 μm). Two neurites criss-cross in box 1. Panels 1a and 2a show the boxed areas in A at higher magnification. Panels 1b and 2b show one of the optical sections from these panels with only the magenta color channel (GluR1) turned on. Panels 1c and 2c merge the TH and GluR1 signals, showing GluR1 on the shaft of a varicose neurite (panel 2c) and on a small, apparently stubby spine (panel 1c). Arrowheads point to identical positions in the panels of each column. (B) Varicose neurites of TH cell (green) in the OPL. The large boxes show higher magnifications of the varicosities outlined in the small boxes, and thin spines attached to each outlined varicosity. Arrows point to other spine-bearing varicosities. Asterisks are next to spine-free varicosities. Scale bar = 20 μm in A; 5 μm in 1c,2c,B

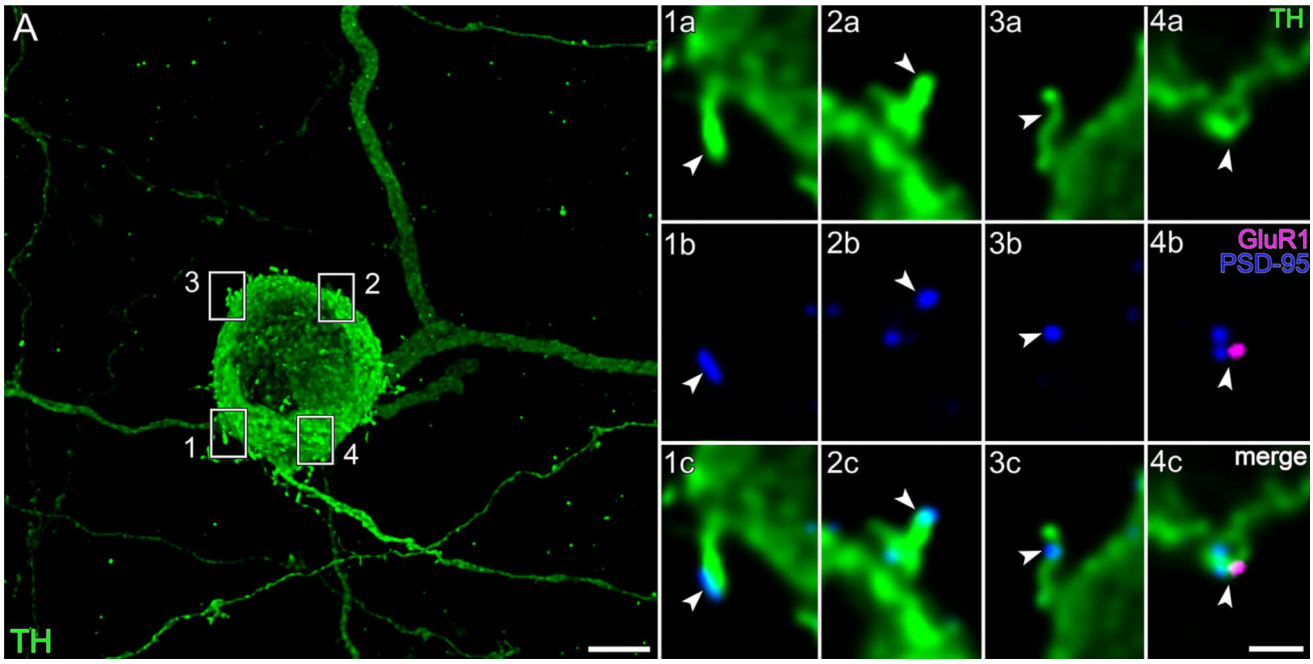

FIGURE 8.

GluR1 and PSD-95. (A) TH cell soma in the GCL, and portions of tapering and varicose neurites, in flat-mounted retina. Z-projection (thickness = 25.92 μm) of optical sections through the proximal IPL and GCL. Areas marked by white boxes are displayed at higher magnification in panels 1a to 4c, one column per box. Each column displays a single optical section, viewed in different color channels. Panels 1a to 4a display TH signal (green). Panels 1b to 4b display GluR1 (magenta) and PSD-95 (blue) signals of corresponding fields. Merges show PSD-95 on the tip and neck of spines in panels 1c to 3c, and colocalization of GluR1 and PSD-95 in panel 4c. Arrowheads point to identical positions in panels of each column. Scale bar = 1 μm in 4c (applies to panels 1a–4c); 5 μm in A

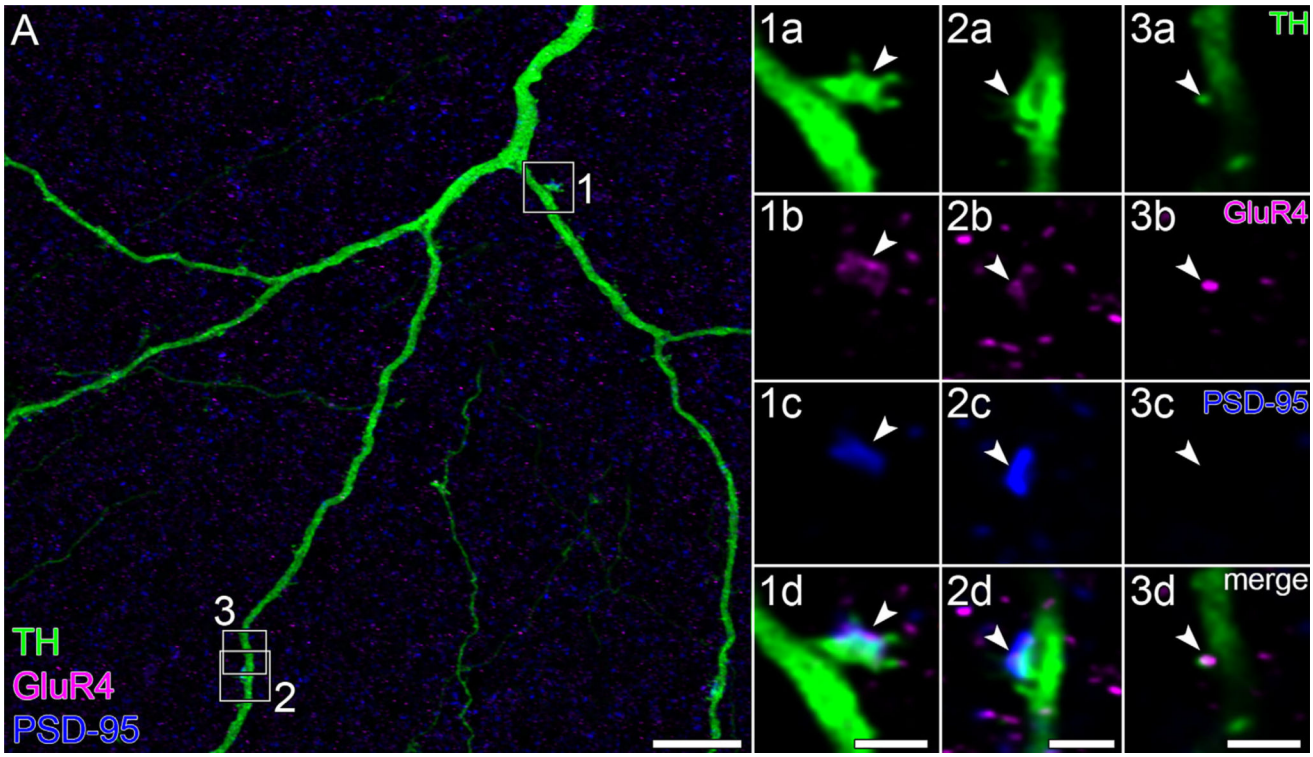

FIGURE 9.

GluR4 and PSD-95. (A) Portions of tapering neurites of TH cell in flat-mounted retina. Z-projection (thickness = 9.8 μm) of optical sections through the proximal IPL. Areas marked by white boxes are displayed at higher magnification in panels 1a to 3d, one column per box. Each column displays a single optical section, viewed in different color channels. Panels 1a to 3a, 1b to 3b, and 1c to 3c display TH (green), GluR4 (magenta), and PSD-95 (blue) signals, respectively. Merges show colocalization of GluR4 and PSD-95 on spines in panels 1d and 2d, and GluR4 on spine in panel 3d. Arrowheads point to identical positions in panels of each column. Scale bars = 2 μm in 1d, 2d, and 3d (apply to 1a–1d, 2a–2d, and 3a–3d, respectively); 10 μm in A.

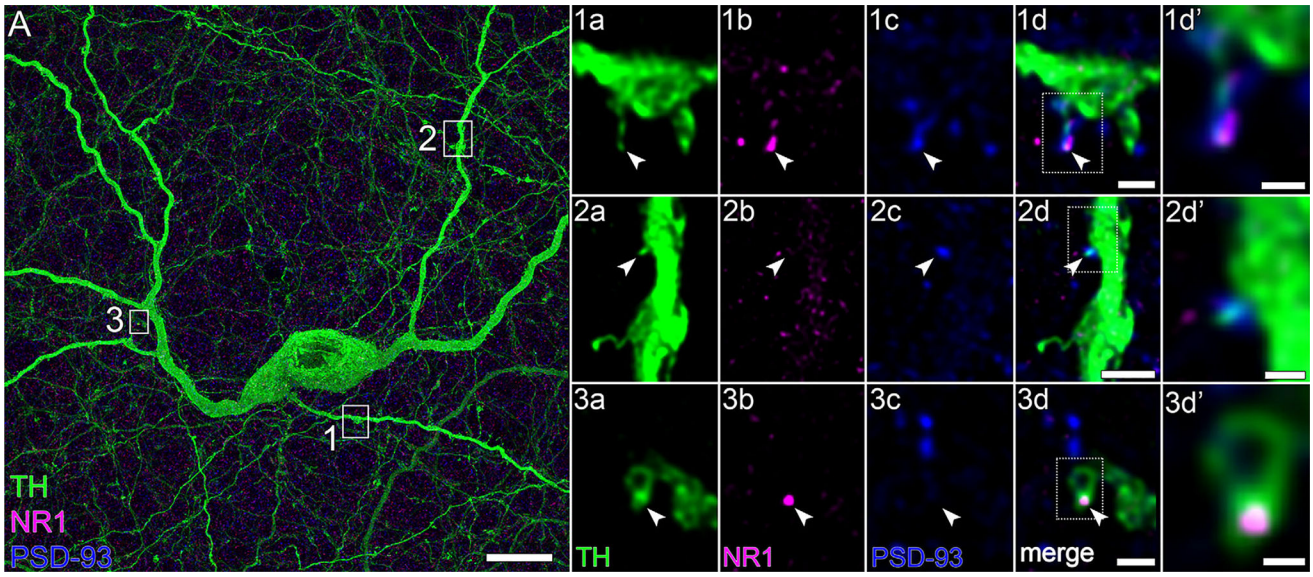

FIGURE 10.

NR1 and PSD-93. (A) TH cell soma (in the INL), and portions of tapering and varicose neurites in flat-mounted retina. The areas marked by white boxes are displayed at higher magnification in panels 1a to 3d′, one row per box. Each row (panels 1a–3d) displays a single optical section, viewed in different color channels. Panels 1a–3a display TH signal (green). Panels 1b–3b and 1c–3c display NR1 (magenta) and PSD-93 (blue) signals, respectively, of corresponding fields. Merges show colocalization of GluR4 and PSD-93 on TH cell thin spine in panel 1d, PSD-93 on stubby spine in panel 2d, and NR1 on nub in panel 3d. Areas marked by dotted-line white boxes in panels 1d–3d are magnified in panels 1d′–3d′, respectively. Arrowheads point to identical positions in panels of each row. Scale bar = 10 μm in A; 1 μm in 1d,3d; 2 μm in 2d; 0.5 μm in 1d′ –3d′

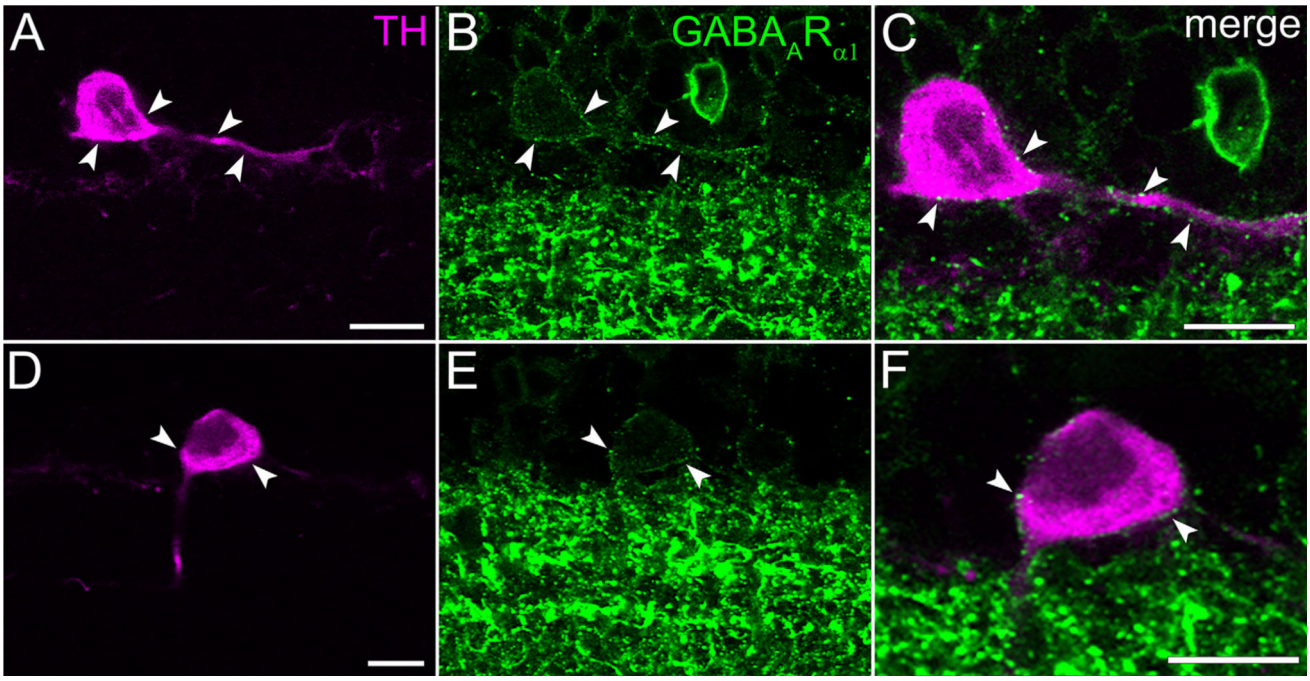

FIGURE 11.

$GABA_AR_{\alpha1}$. (A,D) TH cell soma (in the INL), and portions of tapering neurites in vertical section of retina. Each row displays a single optical section, viewed in different color channels. (A,D) TH signal (magenta). (B,E) $GABA_AR_{\alpha1}$ (green). (C,F) Merges show colocalization of TH and $GABA_AR_{\alpha1}$ on surface of TH cell soma and tapering neurite, especially at arrowheads pointing to identical positions in panels of each row. Scale bar = 10 μm in A,C,D,F (bar in A applies to A,B; bar in D applies to D,E)

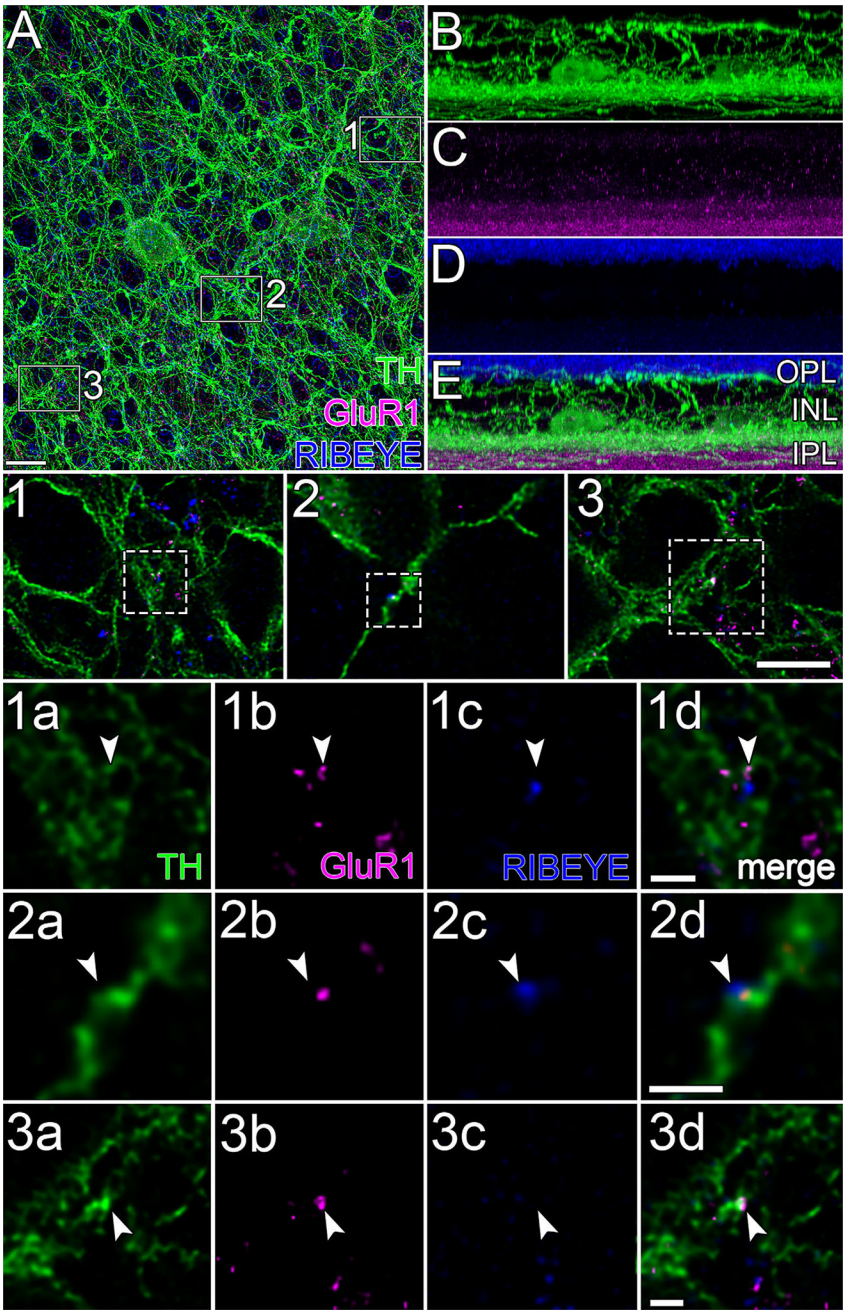

FIGURE 12.

GluR1 and RIBEYE. (A) Projection of 183 optical sections (thickness = 36.56 μm) through the INL and IPL of flat-mounted retina immunostained for TH (green), GluR1 (magenta), and RIBEYE (blue), oversampled, and deconvolved. Note the characteristic TH "rings" formed by TH neurites that surround round, TH-immunonegative areas (Pourcho, 1982; Voigt & Wässle, 1987). Magenta and blue dots within these rings are at different focal planes. (E) 90 ° rotation of A. (B–D) Views of E in each of the color channels. TH cell somata are faint but visible at proximal edge of the INL to the right and left of the center of B. Arborization of TH cell neurites in the OPL, INL, and IPL are more evident than in

Figure 3 due to difference in thickness of tissue displayed. GluR1 signal (C) is heaviest in the proximal IPL but is also present in the distal IPL, INL, and OPL. RIBEYE signal (D) is heaviest at the level of rod axon terminals but is also present in the IPL. Areas marked by boxes in A are displayed at intermediate magnification in panels 1 to 3, and at higher magnification in panels 1a to 3d, one row per box. Each row displays a single optical section, viewed in different color channels. Panels 1a to 3a, 1b to 3b, and 1c to 3c display TH (green), GluR1 (magenta), and RIBEYE (blue) signals, respectively. Merges show apposition of RIBEYE to GluR1 colocalized on TH (1d, 2d) and a colocalization of GluR1 and TH without nearby RIBEYE (3d). Arrowheads point to identical positions in panels of each column. Scale bar = 10 μm in A (applies to A–E); 7 μm in 3 (applies to 1–3); 1 μm in 1d, 2d, and 3d (apply to 1a–1d, 2a–2d, and 3a–3d, respectively)

TABLE 1

Summary of Primary Antibodies

Antibody	Immunogen	Source	Species	Concentration
Anti-TH, RRID: AB_2201528	Tyrosine hydroxylase purified from PC12 cells	Chemicon (#MAB318)	Mouse IgG1, clone LNC1	1:1,000 dilution
Anti-TH, RRID: AB_90755	Native tyrosine hydroxylase from rat pheochromocytoma	Chemicon (#AB1542)	Sheep, polyclonal	1:500 dilution
Anti-GluR1, RRID: AB_2213602	KLH-conjugated linear peptide corresponding to the C-terminal sequence of human glutamate receptor 1	Chemicon (#AB1504)	Rabbit IgG, polyclonal	0.2 μg/ml
Anti-GluR4, RRID: AB_90771	Linear peptide corresponding to the C-terminal sequence (RQSSGLAVIASDLP) of rat glutamate receptor 4	Chemicon (#AB1508)	Rabbit IgG, polyclonal	1 μg/ml
Anti-NR1, RRID: AB_2314955	Synthetic peptide corresponding to amino acids 909–938 of rat NMDAR1 receptor subunit	Chemicon (#AB9864)	Rabbit IgG, clone Rb 1.17.2.6	1:500 dilution
Anti-$GABA_AR_{\alpha 1}$, RRID: AB_310272	KLH-conjugated linear peptide corresponding to the topological domain of rat $GABA_A$ receptor α1 subunit	Upstate Biotechnology (#06-868)	Rabbit IgG, polyclonal	0.5 μg/ml
Anti-PSD95, RRID: AB_2307331	Fusion protein amino acids 77–299 (PDZ domains 1 and 2) of human PSD-95	UC Davis/NIH NeuroMab Facility (#75-028)	Mouse IgG2a, clone K28/43	0.2 μg/ml
Anti-PSD93, RRID: AB_11001825	Fusion protein amino acids 1–852 of rat Chapsyn-110	UC Davis/NIH NeuroMab Facility (#75-284)	Mouse IgG2a, clone N18/28	0.2 μg/ml
Anti-CtBP2, RRID: AB_399431	C-terminal amino acids 361–445 of mouse CtBP2	BD Biosciences (#612044)	Mouse IgG1, clone 16/CtBP2	0.5 μg/ml